AGU PUBLICATIONS

JGR

Journal of Geophysical Research: Biogeosciences

RESEARCH ARTICLE
10.1002/2016JG003716

Key Points:
- Atmospheric CO_2 data are used to estimate several key parameters in a terrestrial ecosystem model using the Global Carbon Assimilation System
- Plants in tropical regions have lower V_{cmax} values than plants in temperate regions. Maximal of V_{cmax} values occur during growing seasons
- We find regular and significant seasonal variation patterns of V_{cmax} and Q_{10} in all latitudinal bands except those in tropical regions

Supporting Information:
- Supporting Information S1

Correspondence to:
J. M. Chen,
jing.chen@utoronto.ca

Citation:
Chen, Z., Chen, J. M., Zhang, S., Zheng, X., Ju, W., Mo, G., & Lu, X. (2017). Optimization of terrestrial ecosystem model parameters using atmospheric CO_2 concentration data with the Global Carbon Assimilation System (GCAS). *Journal of Geophysical Research: Biogeosciences*, *122*, 3218–3237. https://doi.org/10.1002/2016JG003716

Received 15 NOV 2016
Accepted 26 SEP 2017
Accepted article online 30 SEP 2017
Published online 23 DEC 2017

Optimization of Terrestrial Ecosystem Model Parameters Using Atmospheric CO_2 Concentration Data With the Global Carbon Assimilation System (GCAS)

Zhuoqi Chen[1], Jing M. Chen[2,3], Shupeng Zhang[4], Xiaogu Zheng[1], Weiming Ju[2], Gang Mo[3], and Xiaoliang Lu[5]

[1]State Key Laboratory of Remote Sensing Science, College of Global Change and Earth System Science, Beijing Normal University, Beijing, China, [2]International Institute for Earth System Science, Nanjing University, Nanjing, China, [3]Department of Geography & Program in Planning, University of Toronto, Toronto, Ontario, Canada, [4]School of Atmospheric Sciences, Sun Yat-sen University, Guangzhou, China, [5]The Ecosystems Center, Marine Biological Laboratory, Woods Hole, MA, USA

Abstract The Global Carbon Assimilation System that assimilates ground-based atmospheric CO_2 data is used to estimate several key parameters in a terrestrial ecosystem model for the purpose of improving carbon cycle simulation. The optimized parameters are the leaf maximum carboxylation rate at 25°C (V_{max}^{25}), the temperature sensitivity of ecosystem respiration (Q_{10}), and the soil carbon pool size. The optimization is performed at the global scale at 1° resolution for the period from 2002 to 2008. The results indicate that vegetation from tropical zones has lower V_{max}^{25} values than vegetation in temperate regions. Relatively high values of Q_{10} are derived over high/midlatitude regions. Both V_{max}^{25} and Q_{10} exhibit pronounced seasonal variations at middle-high latitudes. The maxima in V_{max}^{25} occur during growing seasons, while the minima appear during nongrowing seasons. Q_{10} values decrease with increasing temperature. The seasonal variabilities of V_{max}^{25} and Q_{10} are larger at higher latitudes. Optimized V_{max}^{25} and Q_{10} show little seasonal variabilities at tropical regions. The seasonal variabilities of V_{max}^{25} are consistent with the variabilities of LAI for evergreen conifers and broadleaf evergreen forests. Variations in leaf nitrogen and leaf chlorophyll contents may partly explain the variations in V_{max}^{25}. The spatial distribution of the total soil carbon pool size after optimization is compared favorably with the gridded Global Soil Data Set for Earth System. The results also suggest that atmospheric CO_2 data are a source of information that can be tapped to gain spatially and temporally meaningful information for key ecosystem parameters that are representative at the regional and global scales.

1. Introduction

Carbon fluxes of terrestrial ecosystems play a key role in regulating atmospheric CO_2 concentrations. There are two common types of method to quantify global distributions of net carbon fluxes. One is atmospheric inversion by utilizing atmospheric CO_2 measurements to inversely estimate the net carbon fluxes (Peylin et al., 2013). Many efforts were devoted to develop individual atmospheric inversion systems (Chevallier et al., 2010; Gurney et al., 2008; Peters et al., 2010; Rayner et al., 2008; Rodenbeck et al., 2003) since the first comprehensive effort dating back to the 1980s (Enting & Mansbridge, 1989; Tans, Conway, & Nakazawa, 1989). This approach deduces spatiotemporal patterns of land/ocean net carbon fluxes at the global scale. However, a disadvantage of the approach is that it cannot provide predictions for the future (Rayner et al., 2005).

The other type of methods is terrestrial biosphere models (TBMs) (Chen et al., 1999; Knorr, 2000; Knorr & Heimann, 2001a, 2001b; Krinner et al., 2005; Potter et al., 1993; Sitch et al., 2003; Wang & Leuning, 1998) that are developed to simulate various physical and biological processes of the biosphere including energy partitioning, photosynthesis, autotrophic and heterotrophic respirations, hydrology, soil heat transfer, etc. An obvious advantage of these models is their ability to make predictions for net carbon fluxes of terrestrial ecosystems in the future (Rayner et al., 2005). However, uncertainties of model parameters are identified as a major limitation of model applications (Green et al., 1999; Luo et al., 2003; Wang, Trudinger, & Enting, 2009). It is necessary to optimize TBM parameters by using observations at the global scale.

Table 1
Prior Values of Default Parameters in BEPS and Their Standard Deviations of for Different PFTs

PFT name	$V_{max,j}^{25}$ [a]	Q_{10}
Broadleaf evergreen	29.0 ± 14.5	2 ± 1
Broadleaf deciduous	57.7 ± 28.5	2 ± 1
Evergreen conifers	62.5 ± 31.0	2 ± 1
Deciduous conifers	39.1 ± 19.5	2 ± 1
Shrub	57.9 ± 29.0	2 ± 1
C4 plants	100.7 ± 50.5	2 ± 1
Others	90.0 ± 45.0	2 ± 1

[a] *j* stands for a specific PFT.

Data assimilation techniques have recently been developed to combine these two common types of method. Through using these techniques, carbon fluxes modeled by a TBM can be optimized using atmospheric CO_2 mole fraction measurements. Some data assimilation systems can also optimize parameters in TBMs using atmospheric CO_2 concentration measurements (Kaminski et al., 2002). The carbon cycle data assimilation system (CCDAS) (Kaminski et al., 2013; Rayner et al., 2005) was a significant development in TBM parameter optimization (Kaminski et al., 2010). In later studies, CCDAS has been extended for use of various types of observation, for example, fPAR (Kaminski, Knorr et al., 2012; Knorr et al., 2010), eddy correlation fluxes (Kato et al., 2013), and satellite-derived atmospheric CO_2 column-averaged volume mixing ratio (Kaminski et al., 2010). Other studies also focused on estimating land surface carbon fluxes (Kaminski, Rayner, et al., 2012; Koffi et al., 2012), constraining TBM parameters (Kaminski et al., 2002; Koffi et al., 2013; Ziehn, Knorr, et al., 2011), and reducing uncertainties (Kuppel et al., 2013; Ziehn, Scholze, et al., 2011; Ziehn et al., 2012) using CCDAS.

Although substantial efforts have been directed toward estimating parameters in TBMs using CO_2 concentration measurements, TBM parameters were optimized as averages for individual plant functional types (PFTs) (Kaminski et al., 2002; Koffi et al., 2013; Ziehn, Knorr, et al., 2011). In addition, seasonal variations of TBM parameters were also rarely discussed at the global scale. In fact, high spatiotemporal variabilities of some key and common parameters were proved at the field scale by many previous studies (He et al., 2014; Mahecha et al., 2010; Wang et al., 2007). To reduce uncertainties of TBMs applied over the globe, it is needed to investigate spatiotemporal variabilities of TBM parameters at the global scale (Ziehn, Knorr, et al., 2011).

This study aims at exploring spatiotemporal variations of TBM parameters using atmospheric CO_2 concentration data through the newly developed Global Carbon Assimilation System (GCAS). GCAS is developed for optimizing global land surface net carbon fluxes and TBM parameters at 1° resolution at weekly time intervals (Chen et al., 2015; Zhang et al., 2014, 2015; Zheng et al., 2014, 2015).

2. Data and Model

2.1. Prediction Model

The prediction model (M) is used to predict a distribution of atmospheric CO_2 concentration (c_t^f) in the tth assimilation window. It contains a TBM (B) with a set of parameters (x_t) and an atmospheric transport model (T). The TBM is employed to estimate net ecosystem productivity (NEP_t) of terrestrial ecosystems in the tth assimilation window. Then the atmospheric transport model is used to predict the distribution of atmospheric CO_2 concentration (c_t^f) with NEP_t, background fluxes (F_t, e.g., ocean fluxes and fossil fuel emissions) in the tth assimilation window, and the distribution of atmospheric CO_2 concentration in the $t-1$ assimilation window (c_{t-1}^a). The prediction model can be written as

$$c_t^f = M(x_t) = T\times(B(x_t) + F_t) + c_{t-1}^a \quad (1)$$

2.2. TBM

The TBM used in this study is BEPS (Boreal Ecosystem Productivity Simulator) (Chen et al., 1999; Ju et al., 2006), which integrates principal processes and mechanisms that are associated with energy partitioning and carbon uptake. BEPS uses leaf-level photosynthetic parameters, such as the maximum carboxylation rate (V_{max}) and the maximum electronic transport rate (J_{max}), to simulate the photosynthesis rates of sunlit and shaded leaves, and the canopy-level GPP is obtained by integrating results from these two leaf groups. It is used to estimate NEP at 1° resolution driven by climate data from NCEP reanalysis data set (Kalnay et al., 1996) for the period from 2000 to 2008. Each grid cell can be made up of any mixture of seven PFTs (Table 1). The PFT named "Others" includes some plant function types that are not listed in the Table 1, such as cropland and grassland. Figure 1 shows the distribution of PFTs with the largest area in each 1° grid and locations of CO_2 concentration observation sites. An area-weighted averaging procedure is followed to

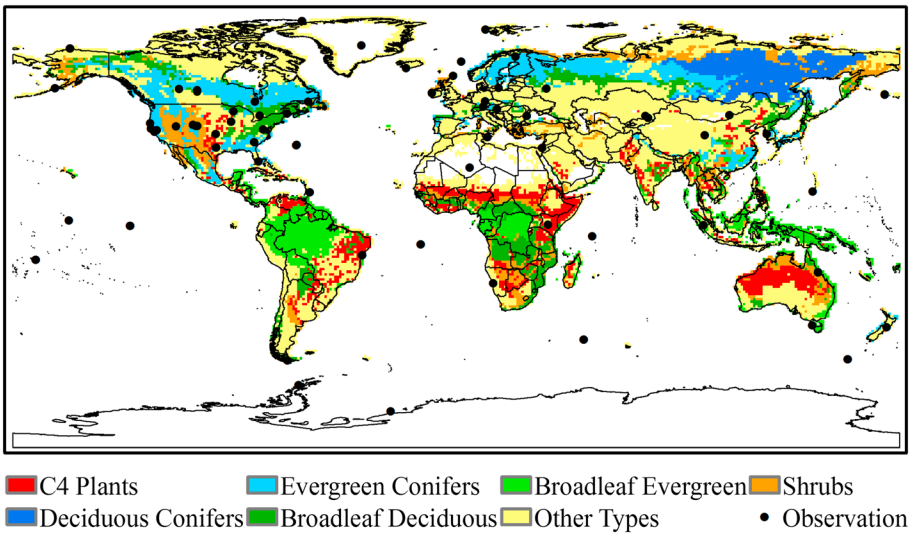

Figure 1. The distribution of plant function types and CO_2 concentration observation sites.

integrate NEPs of seven PFTs for each grid. The detail information about BEPS has been described in previous studies (Chen et al., 2012: Mo et al., 2008). A brief description for BEPS is shown in Text S1 in the supporting information.

2.3. Atmospheric Transport Model

The global chemical transport Model for OZone And Related chemical Tracers (MOZART, Emmons et al., 2010) is used to predict distributions of atmospheric CO_2 concentration at 1° resolution for the period from 2002 to 2008. It is driven by NEPs, background fluxes, a meteorological forcing data set from NCAR reanalysis (Kalnay et al., 1996), and an initial CO_2 concentration distribution. The initial CO_2 concentration distribution at the beginning of the optimization period (2002) was obtained through a 2 year transport model spin-up procedure for the period from 2000 to 2002. The chemistry module of MOZART was closed in the transport simulations for two reasons: (1) data for anthropogenic emissions of all gases that will eventually be converted to CO_2 were insufficient at the global scale, while the consumption of CO_2 by atmospheric chemistry was small, and (2) it helped reduce the computational demand for the high-resolution transport simulations.

2.4. Observations and Background Fluxes

CO_2 measurements include observations of air samples at surface sites and quasi-continuous CO_2 time series from towers. The CO_2 measurements of the period from 2002 to 2008 on 92 sites (Figure 1) were obtained from the ObsPack product (Masarie et al., 2014) distributed through NOAA-ESRL. More than 50,000 CO_2 measurements observed during 12:00–16:00 LST were used in this study. The observation uncertainties were also provided by ObsPack.

Background fluxes contain fossil fuel emissions, ocean fluxes, and fluxes from vegetation fire. The background fluxes are not optimized in GCAS, since the optimized background fluxes from CarbonTracker2013 (CT2013) (Peters et al., 2007, 2010) were selected as inputs to GCAS. The temporal resolution of background fluxes is 3 h. The vegetation fire fluxes were modeled using the Carnegie-Ames-Stanford Approach based on Global Fire Emission Database (van der Werf et al., 2006). The ocean fluxes were from ocean interior pCO_2 inverse estimates recalculated to the air-sea partial pressure difference (Jacobson et al., 2007) and pCO_2-Clim prior estimates derived from the climatology of seawater pCO_2 (Takahashi et al., 2009). The fossil fuel emissions were preprocessed by CarbonTracker2011 from Carbon Dioxide Information and Analysis Center (Marland et al., 2007) and Open-source Data Inventory of Anthropogenic CO_2 emission (Oda & Maksyutov, 2011).

The optimized background fluxes from CT2013 were used as inputs of GCAS, but the land surface fluxes (prior fluxes) used in GCAS and CT2013 were different. These differences caused some substantial deviations of CO_2

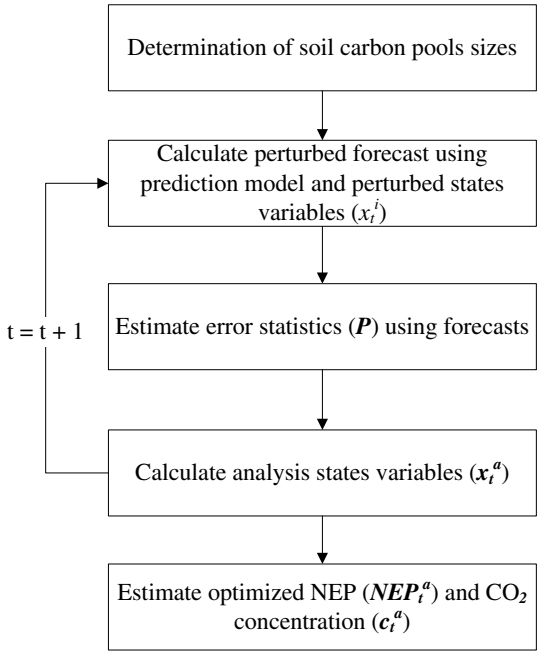

Figure 2. The flowchart of GCAS.

concentration predictions from GCAS and CT2013. A data assimilation system utilizes differences between observations and predictions to optimize the prior fluxes. Therefore, the information used to optimize fluxes and parameters is totally different in GCAS and CT2013. Although optimized background fluxes from CT2013 are used in GCAS, the parameter optimization in GCAS is independent from that in CT2013. Another obvious advantage of using optimized background fluxes from CT2013 is that the errors of the background fluxes had been minimized by CT2013 and can be ignored in GCAS.

2.5. LAI Data

TBM models usually use LAI to calculate the canopy radiation absorption and productivity. In this study, a global LAI product (1981–2008) in 8 day intervals with an 8 km resolution, which was generated by fusion of MODIS and AVHRR data, was used (Liu, Liu, & Chen, 2012). The LAI data were averaged for each PFT type in each 1° modeling grid for the calculation of GPP for each PFT in a grid.

3. GCAS

3.1. Optimized Parameters

GCAS is designed for optimizing parameters in BEPS at 1° resolution using CO_2 concentration measurements. The optimized parameters are the maximum carboxylation rate at 25°C (V_{max}^{25}) for leaf photosynthesis, the temperature sensitivity of heterotrophic respiration (Q_{10}), and the adjustment factor for initial total soil carbon pool sizes (λ). Different optimization strategies are applied to estimate these parameters.

Errors of CO_2 concentration from the prediction model are usually composed of systemic biases and random errors. The systemic biases cause overestimations or underestimations of CO_2 concentration in all prediction steps. The overestimations or underestimations are accumulated over a prediction period, and therefore, they are easily detected in a long period of time (e.g., annual scale). Unlike the systemic biases, positive random errors of the prediction model in a time step may be offset by negative random errors in another step when CO_2 concentration is accumulated in time. The random errors are therefore difficult to detect after a long prediction time. In GCAS, the initial soil carbon sizes are accumulated over thousands of years. They hardly change in a short period. The errors caused by overestimations or underestimations of the initial carbon pool sizes can be accumulated in time. Unlike the errors from the initial carbon pools, errors related to V_{max}^{25} and Q_{10} would offset each other as these two parameters have opposite effects on the net carbon fluxes influencing the atmospheric CO_2 concentrations. Based on above descriptions, the errors related to the initial carbon pool sizes are treated as systemic biases. The errors related to V_{max}^{25} and Q_{10} are considered as random errors.

To correct systemic biases and random errors, a two-step optimization method is developed and used in GCAS. The systemic biases are first corrected by adjusting initial total carbon pool sizes using CO_2 concentration measurements in the last week of the years during the period from 2002 to 2008. The optimized carbon pool sizes are kept constant in the next step. Then the random errors are corrected through using weekly CO_2 concentration measurements to adjust V_{max}^{25} and Q_{10}. The flowchart of GCAS is shown in Figure 2.

3.2. Determination of Initial and Optimized Soil Carbon Pool Sizes

The initial soil carbon pool sizes are determined through a spin-up procedure based on an assumption that C dynamics is approximately in equilibrium before industrialization (Chen et al., 2003). The initial soil carbon pool sizes are set to 0 at the beginning of the spin-up procedure. Then they are accumulated when the BEPS model is running until soil respiration and NPP arrive at the equilibrium. In fact, the C dynamics is not in equilibrium in 2000 due to industrialization. According to Le Quéré et al. (2014), NPP is about 2 PgC larger than heterotrophic respiration in 2000. Therefore, the carbon pool sizes are multiplied by a factor (0.95) so that the global NEP simulated by BEPS is equal to 2 PgC in 2000. Finally, the carbon pools are used as

initial inputs in GCAS to predict CO_2 concentration at 1° resolution from 2002 to 2008. The forecasting procedure can be expressed as follows:

$$c_t^f = M(x_{\mathrm{ini},t}, C) = T\times\left(B(x_{\mathrm{ini},t}, C) + F_t\right) + c_{t-1}^f \tag{2}$$

$$C = (C_1\ C_2\cdots C_9)^T \tag{3}$$

where t represents the tth assimilation window. M, T, and B are the prediction model, MOZART, and BEPS, respectively. $x_{\mathrm{ini},t}$ is a vector containing initial parameters in BEPS. F_t represents the background fluxes. C is a vector of the initial soil carbon sizes. In BEPS, there are nine soil carbon pools, namely, coarse and dead wood detritus pool, surface structural pool, surface metabolic pool, surface microbial pool, fine-root structural litter pool, fine-root metabolic pool, soil microbial pool, slow carbon pool, and passive carbon pool. c_{t-1}^f is the distribution of CO_2 concentration in the $t-1$ assimilation window.

The mismatches between CO_2 concentration measurements and simulations are used to optimize the initial carbon pool sizes through estimating the adjustment factors (λ). The following objective function (equation (3)) is minimized to obtain λ.

$$J(\lambda) = \frac{1}{2}(\lambda\times C - C)^T Q^{-1}(\lambda\times C - C) + \frac{1}{2}(c - M(\lambda\times C))^T (O + P_c)^{-1}(c - M(\lambda\times C)) \tag{4}$$

where λ is a scaling factor at 1° resolution. It is independent of time and the same for all carbon pools in each 1° grid. Q is the error covariance matrix of the initial carbon pools. The standard deviations of the initial carbon pools are set equal to 10% of the initial carbon pool sizes. c is a vector of CO_2 concentration measurements. O is the observation error covariance matrix. P_c is the error covariance matrix of the prediction model. Posterior scaling factors ($\hat{\lambda}$) and carbon pool sizes ($\hat{C}$) can be estimated as

$$C\times\hat{\lambda} = C + \left(QM^T\left(MQM^T + O + P_c\right)^{-1}\right)(c - M(C)) \tag{5}$$

$$\hat{C} = \hat{\lambda}\times C \tag{6}$$

3.3. State Variables

As described by Zhang et al. (2014, 2015), the ensemble Kalman filter was used in GCAS. The length of an assimilation window is set to 1 week. Within the tth week, a vector of the state variables (x_t) contains two parameters of the BEPS model: the maximum carboxylation rate at 25°C for leaf photosynthesis (V_{max}^{25}) and the temperature sensitivity of heterotrophic respiration (Q_{10}).

$$x_t = \left(V_{\mathrm{max},t}^{25}, Q_{10,t}\right) \tag{7}$$

There are up to seven PFTs in every 1° grid cell. It is hard to obtain the optimized V_{max}^{25} values for all PFTs due to limited observations. As an alternative, a base maximum carboxylation rate (V_{base}^{25}) is used in GCAS. The V_{max}^{25} value for a specific PFT can be expressed as a product of V_{base}^{25} and a multiplier (equation (8a))

$$V_{\mathrm{max},j}^{25} = \beta_j\times V_{\mathrm{base}}^{25} \tag{8a}$$

$$\beta_j = V_{\mathrm{max},j}^{25}/V_{\mathrm{base}}^{25} \tag{8b}$$

j denotes the jth PFT. The multiplier (β_j) makes the $V_{\mathrm{max},j}^{25}$ value equal to initial value shown in Table 1. It can be calculated as equation (8b) before implementing GCAS. Then β_j is treated as constants in GCAS. There are seven multipliers that are corresponding to seven PFTs. The multipliers are not optimized in GCAS. V_{base}^{25} is initially set to 50 μmol m^{-2} s^{-1}. It is optimized in every assimilation window in GCAS. Then the optimized $V_{\mathrm{max},j}^{25}$ is derived following equation (8b) by applying the multipliers β_j to optimized V_{base}^{25}.

Therefore, the state vector in the tth assimilation window can be written as

$$x_t = \left(V^{25}_{\text{base},t}, Q_{10,t}\right) \tag{9}$$

About 26,000 parameters are estimated in an assimilation window.

3.4. Calculate Perturbed Forecasts and Forecast Errors

The perturbed CO_2 concentration forecasts are obtained using the prediction model (M) with perturbed state vectors. It can be expressed as

$$c^f_{t,i} = M\left(x^i_t\right) = T\times\left(B\left(x^i_t\right) + F_t\right) + c^a_{t-1} \tag{10}$$

where x^i_t is the ith member of the perturbed state vectors in tth assimilation window. The total number of ensemble members is 50. A random perturbation technique is applied to generate the ensemble state vectors in every assimilation window. The ensemble parameters are sampled from Gaussian distributions with prior mean values (x^m) and prior standard deviations at the beginning of the optimization (Table 1). Then, x^m and the standard deviations are taken from the analysis state in the last assimilation window. $c^f_{t,i}$ is the ith ensemble member of CO_2 concentration predictions in the tth assimilation window. M is the prediction model with the state vector x^i_t. c^a_{t-1} is the optimized distribution of CO_2 concentration in the $t-1$ assimilation window.

The error covariance matrix (P) of the prediction model is estimated as

$$p = \left(M\left(x^1_t\right) - M(x^m), M\left(x^2_t\right) - M(x^m), \cdots M\left(x^n_t\right) - M(x^m)\right) \tag{11}$$

$$P = \frac{p\times p^T}{n-1} \tag{12}$$

where n is the total ensemble number. Because only one transport model is used in GCAS, the transport uncertainty is not explicitly evaluated. However, the forecast error of the prediction model is estimated using the perturbed states vectors, and therefore, the transport uncertainty is included as a part of the forecast error to consider its influence on the parameter optimization.

3.5. Calculate the Analysis State

In the tth assimilation window, the following objective function (equation (13)) is minimized to obtain the optimized state vector (x^a_t) and postparameter uncertainties (R_{post}).

$$J(x) = \frac{1}{2}\left(x - x^m_t\right)^T R^{-1}\left(x - x^m_t\right) + \frac{1}{2}(c - M(x))^T(O+P)^{-1}(c - M(x)) \tag{13}$$

$$x^a_t = x^m_t + R\mathrm{M}^T\left(\mathrm{M}R\mathrm{M}^T + O + P\right)^{-1}\left(c - M\left(x^m_t\right)\right) \tag{14}$$

$$R_{\text{post}} = R - R\mathbf{M}^T\left(\mathbf{M}R\mathbf{M}^T + O + P\right)^{-1}\mathbf{M}R \tag{15}$$

$$M = \left.\frac{\partial M}{\partial x}\right|_{x=x^m_t} \tag{16}$$

where x^a_t is the optimized state vector at 1° resolution, R is the error covariance matrix of the prior model parameters, c is a vector of CO_2 concentration measurements, O is the error covariance matrix of observations that is built based on the observation uncertainty from ObsPack, and P is the error covariance matrix of the prediction model. The finite difference method is used to estimate M. The uncertainty reduction rate is defined as

$$E(\%) = \left(1 - {}^{R_{\text{post}}}\!/_{R}\right)\times 100 \tag{17}$$

Then BEPS with the optimized state vector (x^a_t) is used to estimate optimized NEP (NEP^a_t). The optimized distribution of CO_2 concentration (c^a_t) is also estimated by using the prediction model driven by optimized NEP and background fluxes, as follows:

Table 2
Annual NEPs (unit: PgC yr^{-1}) Estimated by BEPS, GCAS, and CT2013 for the Period From 2002 to 2008

Year	BEPS	GCAS	CT2013
2002	2.02	2.33	2.97
2003	2.16	2.66	3.00
2004	2.05	2.63	4.52
2005	0.61	1.44	3.17
2006	1.05	2.10	4.30
2007	0.84	2.36	3.88
2008	1.58	2.60	4.68
Average	1.47	2.20	3.79

Note. The BEPS model was driven by the default parameters shown in Table 1.

$$\mathrm{NEP}_t^a = \mathrm{BEPS}\left(x_t^a\right) \tag{18}$$

$$c_t^a = M\left(B\left(x_t^a\right) + F_t\right) + c_{t-1}^a \tag{19}$$

4. Results

4.1. NEP

The results of optimized NEP by GCAS are summarized in Table 2. The NEP results from CT2013 (Peters et al., 2007) are also shown for comparison with the results from GCAS. The average annual NEP values from 2002 to 2008 estimated by the two data assimilation systems are all greater than the value from BEPS with default parameters shown in Table 1 (1.47 PgC yr^{-1}). The value from CT2013 is the largest (3.79 PgC yr^{-1}) among all systems, while the value by GCAS is 2.20 PgC yr^{-1}. The differences between GCAS and CT2013 are probably more related to the prior net carbon fluxes from land surface models. Although the average annual NEP estimated by CT2013 is about twice as large as the value from GCAS, interannual variabilities of NEPs from these two systems are similar. For instance, less/more carbon uptake in 2005/2008 is observed by both GCAS and CT2013.

The distributions of the average annual NEP estimated by BEPS, GCAS, and CT2013 are shown in Figure 3. BEPS, GCAS, and CT2013 exhibit a large carbon uptake over the northern hemisphere and tropical areas. GCAS and BPES display weaker carbon uptake than CT2013 in most areas. Many significant differences between BEPS/GCAS and CT2013 are discovered in the southern part of South America, Eurasia boreal regions, North America boreal regions, etc. GCAS and BEPS show a carbon sink over the southern part of South America, while a carbon source is produced in CT2013. The carbon sinks from GCAS over Eurasia boreal regions and America boreal regions are much weaker than the sinks from CT2013. Some spatial patterns of NEP are also somewhat different between the results from GCAS and CT2013, such as those over Australia and South America. The spatial pattern of NEP from GCAS is similar to that from BEPS. However, GCAS also makes many substantial changes over BEPS. For example, GCAS enhanced carbon sinks over Eurasia boreal regions and tropical regions. These changes are supported by CT2013.

Figure 4 displays the zonal mean NEP for BEPS, GCAS, and CT2013 over the period from 2002 to 2008. BEPS and GCAS display carbon sinks over midlatitude regions of the southern hemisphere. Due to negative NEP values produced over the southern part of South America (Figure 3), CT2013 shows a carbon source over midlatitude regions of the southern hemisphere. Compared with the fluxes estimated by BEPS, both CT2013 and GCAS increase NEP over tropical regions (20°S–20°N). BEPS, GCAS, and CT2013 have good agreement in midlatitudes of the northern hemisphere. In high-latitude regions of the northern hemisphere, GCAS is consistent with BEPS and produces lower sinks than the sinks from CT2013. A large carbon uptake is produced by CT2013 over high-latitude regions of the northern hemisphere, especially over Eurasia boreal regions (Figure 3), such as Russia. NEPs from BEPS, GCAS, and CT2013 are 0.24, 0.31, and 1.08 PgC yr^{-1} over Russia, respectively. An independent study of Dolman et al. (2012) used three methods based on forest inventory, eddy covariance carbon flux measurements, and atmospheric inversion to estimate the net carbon flux over Russia. Their results suggested that the average carbon uptake from the three methods is about 0.61 PgC yr^{-1}. The carbon uptake estimates range from 0.34 to 1.35 PgC yr^{-1}. The result from GCAS is close to the lower boundary of these estimates, while the result from CT2013 is close to the upper boundary. These large uncertainties of NEPs from different systems and studies may be due to the lack of CO_2 concentration observations in this region.

Land surface fluxes retrieved from inversion and data assimilation systems often differ substantially, due to different choices for the spatial/temporal flux resolution, prior fluxes, transport models, and observational constraints (Gurney et al., 2004). It is useful to assess the results from GCAS by comparing with the results of other atmospheric CO_2 inversion systems. Eleven atmospheric CO_2 inversion systems used by Peylin et al. (2013) are selected to compare with GCAS. The results from the inversion systems were obtained from network (http://transcom.lsce.ipsl.fr/). The values of "Fossil-corrected Natural Fluxes" from 1996 to 2008 were read from "bar plots" published in the website. "Natural Fluxes" are defined as total fluxes minus fossil fuel emissions. To transform NEP to "Natural Fluxes," the NEP values from CT2013 and GCAS are subtracted by

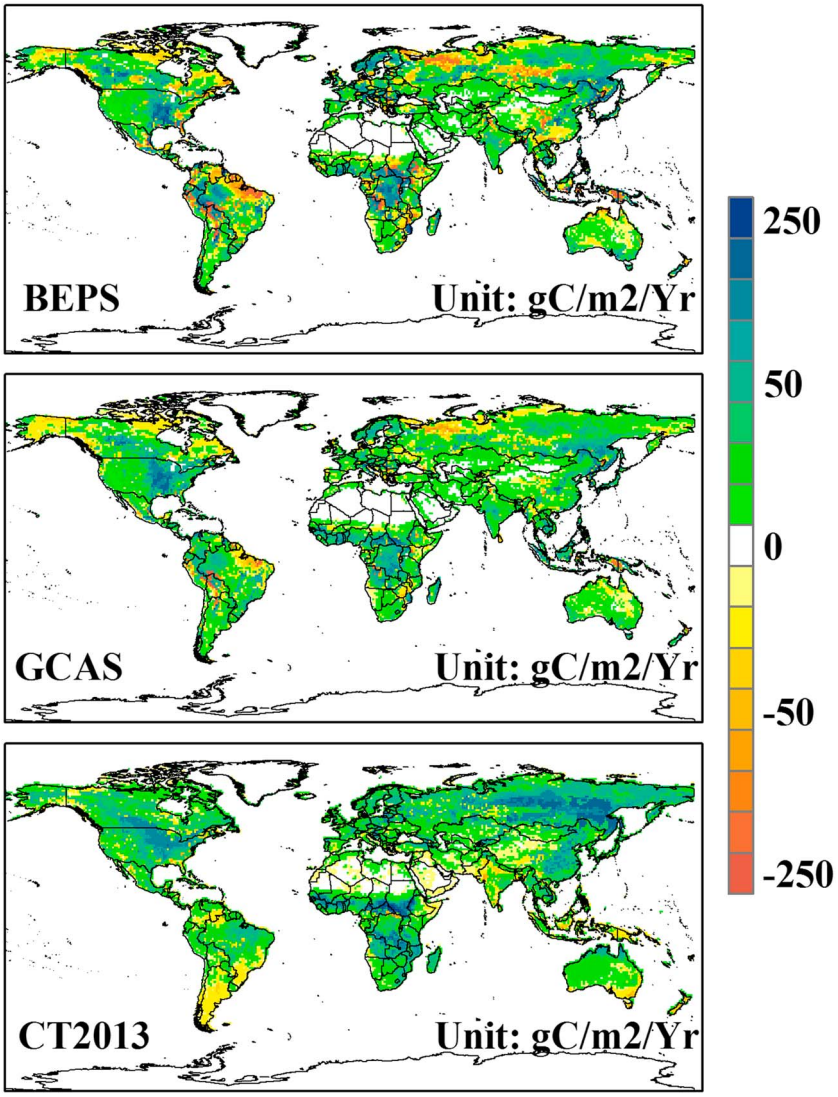

Figure 3. The distribution of average annual NEP (unit: gC m^{-2} yr^{-1}) estimated by different systems for the period from 2002 to 2008. (a) NEP from BEPS with default parameters shown in Table 1. (b) Optimized NEP from GCAS. (c) Optimized NEP from CT2013.

the vegetation fire fluxes provided by CT2013 (Peters et al., 2007; van der Werf et al., 2006). Although the time period of the results of Peylin et al. (2013) is longer than that of GCAS and CT2013, the terrestrial sink has only a weak increasing trend from 1996 to 2008 (Le Quere et al., 2013). The comparison of the 7 year mean values of GCAS and CT2013 and the 13 year mean values of Peylin et al. (2013) within the period from 1996 to 2008 period is therefore meaningful.

The boxes in Figure 5 present minimum and maximum extents of the natural carbon fluxes from the CO_2 inversion systems. The horizontal lines in the boxes display the mean natural fluxes of the inversion systems. The natural fluxes by GCAS fall into the ranges of the fluxes from the inversion systems. The results of GCAS are similar to those of CT2013 except over Eurasia boreal regions. CT2013 indicates a large carbon sink, while a moderate carbon uptake is produced by GCAS. Figure 5 therefore shows that the optimized NEPs from GCAS are comparable to the ensemble means of the inversion results for most regions.

4.2. Error Analysis

BEPS is run with default parameters shown in Table 1 and optimized parameters from GCAS to estimate prior NEPs and optimized NEPs, respectively. These NEP fields and the background fluxes are used to force MOZART

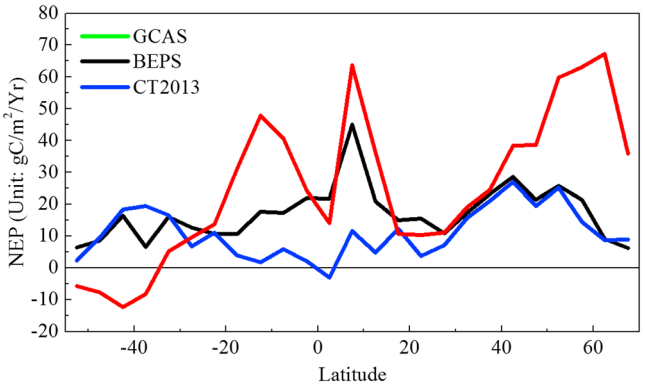

Figure 4. Zonal mean NEPs (unit: gC m^{-2} yr^{-1}) from different systems for the period from 2002 to 2008 in different latitudinal bands. The blue line presents NEPs estimated by BEPS with default parameters shown in Table 1. The black line presents NEPs estimated by GCAS. The red line presents NEPs estimated by CT2013.

to simulate daily CO_2 concentrations for the period from 2002 to 2008. The simulated atmospheric CO_2 concentrations are evaluated by measurements (Figure 6a). The RMSE between simulated and observed concentrations is significantly reduced from 4.67 to 3.43 ppm when optimized NEPs are used. Then the prediction model was driven by NEPs from BEPS, GCAS, and CT2013 to predict CO_2 concentrations for the period from 2005 to 2008. The predictions were compared with independent observations of CO_2 concentration from the comprehensive observation network for trace gases by airliner (CONTRAIL). The RMSEs for the predictions from the prediction model driven by NEPs from BEPS, GCAS, and CT2013 are 5.03, 3.96, and 1.91 ppm, respectively (Figure 6b). Although the RMSE value for GCAS is larger than that for CT2013, the results suggest that the performance of BEPS with optimized parameters is substantially better than that with default parameters.

Chi-square statistics (χ^2) are usually used to test the error covariances or the innovations in a data assimilation system (Zhang et al., 2015; Zupanski & Zupanski, 2006). For the tth time step, it is defined as

$$\chi^2 = \frac{1}{N_{\text{obs}}}\left(c_t - M\left(x_t^m\right)\right)^T \left(\frac{1}{n-1}\mathbf{M}R_t\mathbf{M}^T + O_t + P_t\right)^{-1}\left(c_t - M\left(x_t^m\right)\right) \quad (20)$$

where N_{obs} is the number of observations. If χ^2 follows a chi-square distribution, its mean value and variance of should be close to 1 and 2. If χ^2 departs significantly from the value of 1, it indicates the divergence of the filter. χ^2 values of GCAS range from 1 to 2.5 with a mean of 1.53 (Figure 7). It is reasonable and consistent with the results from GCAS without error inflations (Zhang et al., 2015). A clear seasonality of χ^2 can be found in Figure 7. The χ^2 values are always larger in northern summer than in northern winter. The seasonality of χ^2 may be caused by either the differences between observations (C_t in equation (20)) and forecasts ($M\left(x_t^m\right)$ in equation (20)) or errors (R, O_t, and P_t in equation (20)) in GCAS, since the χ^2 value is a ratio between the differences and the errors (equation (20)). χ^2 values are always larger than 1 in Figure 7 because the errors estimated in GCAS are less than the differences between observations and forecasts. The global carbon sinks from both observations and forecasts in northern winter are much less than the sinks in northern summer. Then the deviations of forecasts from observations are commonly smaller in northern winter than in northern summer. In addition, due to the small ensemble size in GCAS, the prediction errors may be underestimated. Since the uncertainties are usually related to the magnitude of carbon fluxes, GCAS may have more underestimation of the prediction errors in northern summer than in northern winter. Therefore, the χ^2 values are commonly larger in northern summer than in northern winter in GCAS (Figure 7). There are some ways to help reduce errors in a data assimilation system. Our previous results showed that the inflations on forecast errors and observation errors applied to GCAS can improve the estimation of error statistics (Zhang et al., 2015). Furthermore, more observations used or control variables optimized in a data assimilation system also can help reduce the errors (Zupanski & Zupanski, 2006).

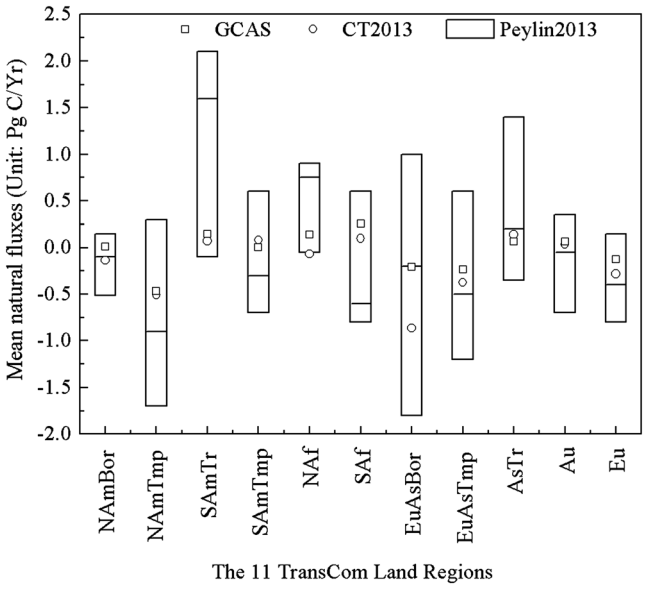

Figure 5. Average annual natural fluxes (in PgC/yr^{-1}) from different systems for the Transcom land regions. The squares show values of average annual natural fluxes from GCAS. The circles show values of average annual natural fluxes from CT2013. The boxes show minimal and maximal values of average annual neutral fluxes from 11 inversion systems (Peylin et al., 2013). The horizontal lines in the boxes are mean annual natural fluxes of 11 inversion systems. The TransCom land regions are Boreal North America (NAmBor), Temperate North America (NAmTmp), Tropical South America (SAmTr), Temperate South America (SAmTmp), North Africa (NAf), South Africa (SAf), Boreal Eurasia (EuAsBor), Temperate Eurasia (EuAsTmp), Tropical Asia (AsTr), Australia (Au), and Europe (Eu), respectively.

4.3. Optimized Soil Carbon Pool Sizes

A gridded Global Soil Data Set for Earth System models (GSDE, Figure 8a) (Shangguan et al., 2014) developed based on soil databases and soil maps is selected as a reference data to be compared with the initial

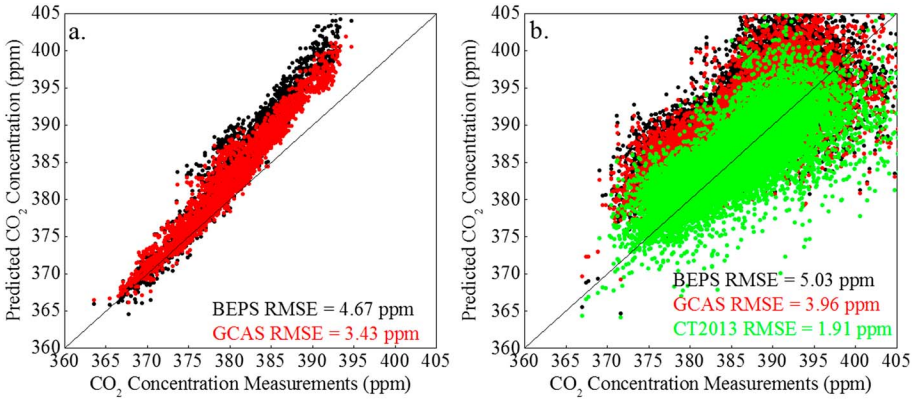

Figure 6. Comparison between CO_2 concentration measurements with simulations. (a) The site measurements were predicted by the prediction model driven by NEPs from BEPS and GCAS during the period from 2002 to 2008. (b) The contrail measurements were predicted by the prediction model driven by NEPs from BEPS, GCAS, and CT2013 during the period from 2005 to 2008. The BEPS model was driven by the default parameters shown in Table 1.

and optimized soil carbon pool sizes. The soil carbon pool sizes from GSDE are large over high latitudes of the northern hemisphere and small over the arid and semiarid areas. The distribution of initial soil carbon pool sizes (ISCD) from BEPS is shown in Figure 8b. It also depicts similar spatial patterns as GSDE. However, many differences between GSDE and ISCD are also detected. For instance, ISCD gives higher values than GSDE in the eastern America, boreal Europe regions, the southern China, and tropical regions of South America. The distribution of the ratio between GSDE and ISCD indicates that magnitudes of GSDE are more/less than 1.2/0.8 times of ISCD in most regions of the world (Figure 8c). The possible explanation is that spatial scale of GSDE and ISCD are different. GSDE is retrieved from field measurements at a fine scale (about 10 km), while ISCD is obtained at 1° resolution. Although magnitudes of the soil carbon density from ISCD and GSDE are quite different, GSDE implies overestimations and underestimations of soil carbon pool sizes in ISCD. The spatial pattern of the adjustment multipliers for ISCD (λ, equation (4)) derived by GCAS is shown in Figure 8d. The spatial scale of the adjustment multipliers is also different from GSDE. It is not surprising that magnitudes of the adjustment multipliers are significantly smaller than the ratios between GSDE and ISCD. However, the distribution of the adjustment multipliers is supported by the ratio. For example, the adjustment multipliers are less than 1 over North America and western regions of boreal Europe where GSDE is less than ISCD. These results suggest that GCAS effectively utilizes information in CO_2 concentration measurements to improve ISCD.

4.4. Global Parameterization of V_{base}^{25}

Figure 9 shows the distribution of optimized multiyear average V_{base}^{25} derived from GCAS for the period from 2002 to 2008. The optimized V_{base}^{25} values range from 49 to 51 μmol m^{-2} s^{-1} over most regions of the world. Larger V_{base}^{25} values are found over temperate regions, such as southeast U.S.A. and southern China. Although the optimized multiyear average V_{base}^{25} values over tropical regions are close to the values over high-latitude regions, the seasonal variability of V_{base}^{25} is stronger in high-latitude regions than in tropical or low-latitude regions (Figure 10). In high-latitude regions, the key characteristic of the seasonal variation of V_{base}^{25} is that the maximum in V_{base}^{25} occurs during a growing season, while the minimum in V_{base}^{25} appears during a nongrowing season. In tropical regions, optimized V_{base}^{25} values keep about 50 μmol m^{-2} s^{-1} all year round. Seasonal fluctuation in V_{base}^{25} becomes strong with increasing latitude. The possible explanations for the seasonal variations of the derived V_{max}^{25} will be discussed in section 5.

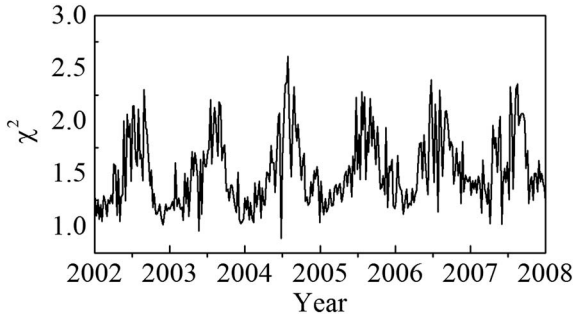

Figure 7. Weekly chi-square (χ^2) statistics of error covariance of GCAS for all CO_2 concentration observations from 2002 to 2008. The mean and standard deviation of χ^2 are 1.53 and 0.33.

The distribution and histogram of optimized multiyear average V_{max}^{25} for broadleaf deciduous forests are shown in Figure 11. Higher V_{max}^{25} values

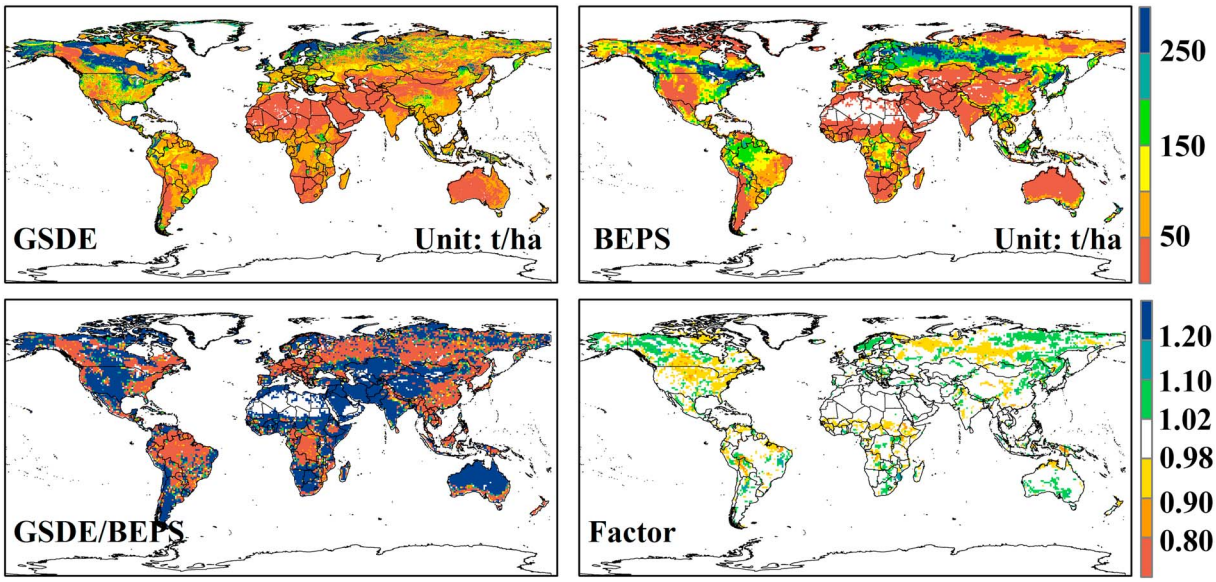

Figure 8. The distribution of soil carbon density (unit: t/ha) and adjustment factors. (a) Reference soil carbon density from observations (GSDE, Shangguan et al., 2014). (b) Initial soil carbon density (ISCD) used by BEPS. (c) Rations between GSDE and ISCD. (d) Mean values of adjustment multiplier (λ) for ISCD retrieved by GCAS for the period from 2002 to 2008.

are found over the southeast of North America and the tropical Asia. The distribution of V_{max}^{25} (Figure 11a) suggests that V_{max}^{25} values are quite variable spatially. They are not simply dependent on a specific PFT as described in TBMs. The histogram of optimized V_{max}^{25} values for broadleaf deciduous forests follow a Gaussian distribution with a mean of 57.4 μmol m^{-2} s^{-1} and a standard deviation of 3.68 μmol m^{-2} s^{-1} (Figure 11b). Histograms of optimized V_{max}^{25} values for other PFTs also follow Gaussian distributions. Mean values of optimized V_{max}^{25} for C4 plants, evergreen conifers forests, deciduous conifers forests, broadleaf evergreen forests, shrubs, and other types plants are 100.3, 62.5, 39.1, 28.8, 57.6, and 89.7 μmol m^{-2} s^{-1}, respectively, and their corresponding standard deviations are 9.73, 2.05, 0.61, 1.39, 2.56, and 5.91 μmol m^{-2} s^{-1}, respectively.

4.5. Global Parameterization of Q_{10}

Figure 12 shows the spatial pattern of multiyear average Q_{10} derived from GCAS for the period from 2002 to 2008. The optimized Q_{10} values vary from 1.95 to 2.05 over most regions of the world. Relatively high Q_{10} values are derived over middle and high-latitude regions where annual average temperature is lower than

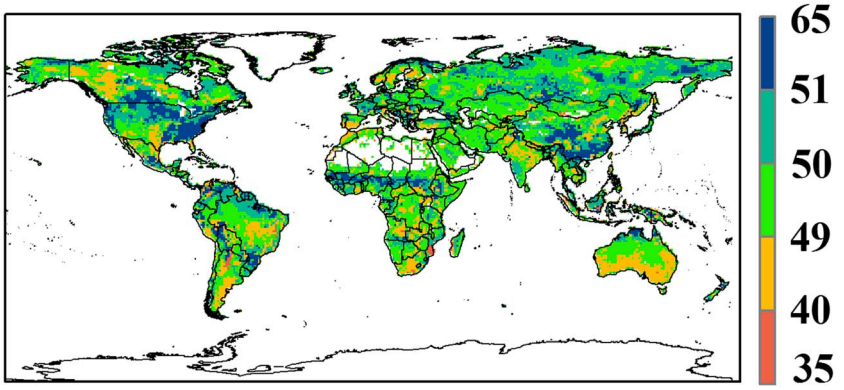

Figure 9. The distribution of the average of weekly optimized V_{base}^{25} (unit: μmol m^{-2} s^{-1}) estimated by GCAS for the period from 2002 to 2008.

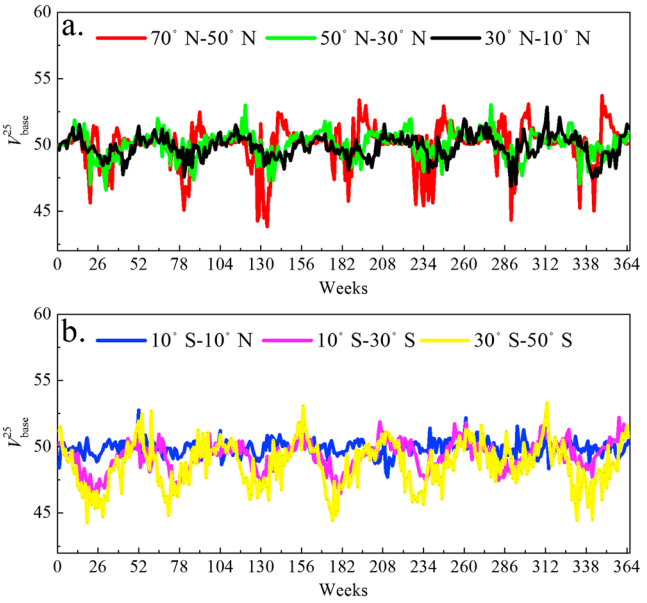

Figure 10. Time series of zonal mean of optimized weekly V^{25}_{base} (in μmol m^{-2} s^{-1}) in different latitudinal bands during the period from 2002 to 2008.

other regions. An exception is that a center with low Q_{10} values appears over Eurasia regions where annual average temperature is also low. The center with low Q_{10} values is also found by Zhou et al. (2009).

The optimized Q_{10} shows stronger seasonal variability in high-latitude regions than in tropical or middle latitude regions (Figure 13). Time series of optimized Q_{10} suggest that Q_{10} values change little all year round over tropical regions, while their seasonal fluctuations become larger at higher latitudes. Seasonal variation in Q_{10} is probably related to the variation in temperature. For instance, the highest Q_{10} value is observed in winter, while the lowest Q_{10} value is found in summer over high-latitude regions (red and yellow line shown in Figure 13). The seasonal variation patterns of Q_{10} shown in Figure 13 confirm the conclusions drawn by Kirschbaum (1995, 2010), who indicated that the temperature dependence of organic matter decomposition is greater at lower temperatures.

There are two types of methods for estimating Q_{10} from observations. One type estimates apparent Q_{10}, which is the temperature sensitivity of ecosystem respiration controlled by environmental factors. Another type derives intrinsic Q_{10}, which represents the unconfounded temperature sensitivity of ecosystem respiration. Mahecha et al. (2010) argued that intrinsic Q_{10} values for ecosystem respiration show global convergence to small values (about 1.4), while apparent Q_{10} values have large variabilities (0.21 to 5.65, see supporting information (S4) in Mahecha et al., 2010). In fact, most studies including this work could not minimize the influence of confounding environmental effects. Apparent Q_{10} is retrieved usually. Q_{10} values derived from field observations usually varied in a range of almost one order of magnitude (Janssens & Pilegaard, 2003; Lloyd & Taylor, 1994; Mahecha et al., 2010). The spatiotemporal distributions of the optimized Q_{10} confirm to the existing understanding of its geographical and seasonal patterns. These results could not be obtained from averaging limited site data and therefore have credibility for regional ecosystem modeling. This successful exploration in using the CO_2 concentration in this way may open doors for further investigations of the spatiotemporal behavior of this important parameter when more atmospheric CO_2 data become available.

4.6. Uncertainty Reduction

The distributions of uncertainty reduction rate for V^{25}_{max} and Q_{10} in northern winter (31 January 2002) and summer (1 August 2002) are shown in Figure 14. The uncertainty reduction rates for V^{25}_{max} and Q_{10} range from 20% to 40% and from 30% to 50%, respectively. The rates for V^{25}_{max} in northern winter and summer are quite different. In northern winter, the rates for V^{25}_{max} are close to zero over middle and high-latitude regions of the north hemisphere, while they significantly increase in northern summer. The rates for V^{25}_{max} are about 30%

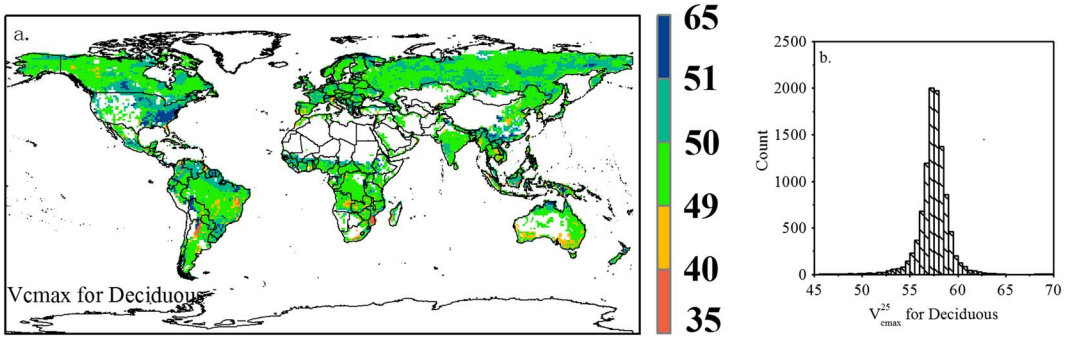

Figure 11. The distribution and histogram of multiyear average weekly optimized V^{25}_{max} (unit: μmol m^{-2} s^{-1}) for broadleaf deciduous forest from 2002 to 2008. (a) The distribution of multiyear average weekly optimized V^{25}_{max} for broadleaf deciduous forest. (b) The histogram of multiyear average weekly optimized V^{25}_{max} for broadleaf deciduous forest.

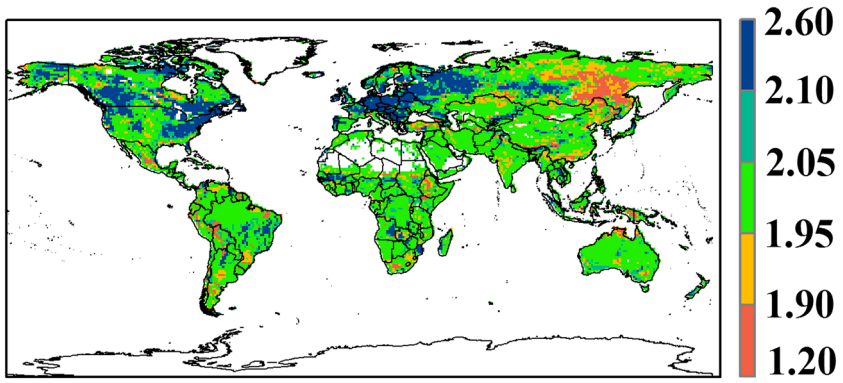

Figure 12. The distribution of average of weekly Q_{10} values estimated by GCAS for the period from 2002 to 2008.

over tropical regions both in northern summer and winter. The distributions of uncertainty reduction rates for Q_{10} in northern summer and winter are similar. The rates for Q_{10} over tropical regions are larger than over middle and high latitudes. Uncertainty reduction rates over regions with dense observation networks are not larger than the rates over regions with sparse observation networks. However, a dense observation network provides more detail information about the distribution of uncertainty reduction rates. For example, the uncertainty reduction rates for Q_{10} over tropical regions with a sparse observation network are much larger than the rates over regions with a dense observation network (e.g., North America and Europe), while the distribution of the rates over North America and Europe is more complex than the distribution over tropical regions (Figures 14c and 14d). The rates of uncertainty reduction for different seasons were also calculated and shown in Figure S1 in the supporting information. The distributions of seasonal reduction rates are similar to the distributions of the rates for two specific dates.

5. Discussions

5.1. Global Distribution and Seasonal Variation of V_{max}^{25}

The leaf-level photosynthesis calculation scheme proposed by Farquhar et al. (1980) has been widely used by TBMs. V_{max}^{25} is a key parameter in Farquhar's scheme. Many efforts have been made to investigate photosynthetic capacity based on a large number of species (De et al., 2015; Niinemets et al., 2015; Medlyn et al., 1999; Reich et al., 2007; Wilson et al., 2000]. However, due to high variability of V_{max}^{25} (Medlyn et al., 2002), it is difficult to describe the spatial pattern of V_{max}^{25} on the global scale. In this study, we explore V_{max}^{25} values at the global scale through the GCAS system. The key finding about the distribution of V_{max}^{25} is that plants from tropical regions have lower V_{max}^{25} values than plants from temperate regions. The result is consistent with Kattge et al. (2009) and Ali et al. (2015). A possible explanation is that plants from temperate regions have higher nitrogen use efficiency than plants from tropical regions (Ali et al., 2015). Other studies supposed that V_{max}^{25} values that increase with latitude could be acclimation of plants to environment factors. (Hikosaka et al., 2006; Kattge & Knorr, 2007; Yamori et al., 2005).

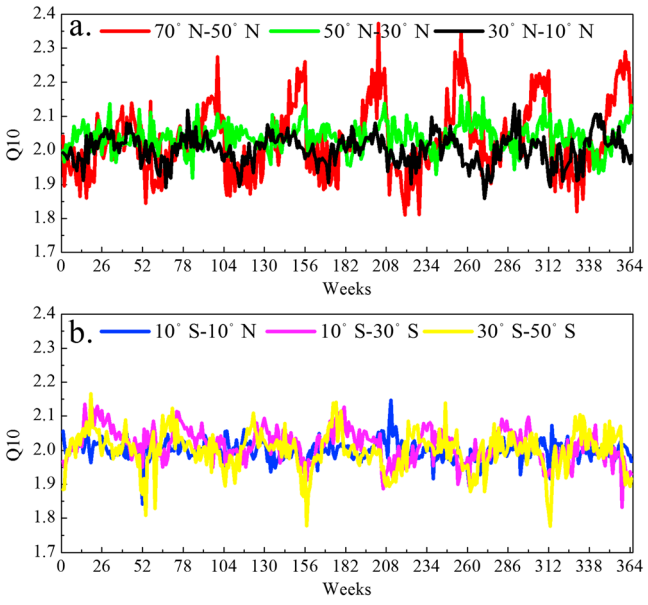

Figure 13. Time series of zonal mean of optimized weekly Q_{10} values in different latitudinal bands for during the period from 2002 to 2008.

Previous studies observed seasonal fluctuations of V_{max}^{25} in some specific plants (Croft et al., 2015; Grassi et al., 2002; Wang et al., 2007; Wilson et al., 2000). It is hard to describe the seasonal variation patterns of V_{max}^{25} at the global scale based on sites observations. This study finds regular and significant seasonal variation patterns of V_{max}^{25} in all latitudinal bands except those in tropical regions. Maximal V_{max}^{25} values occur during growing seasons, while minimal values occur during

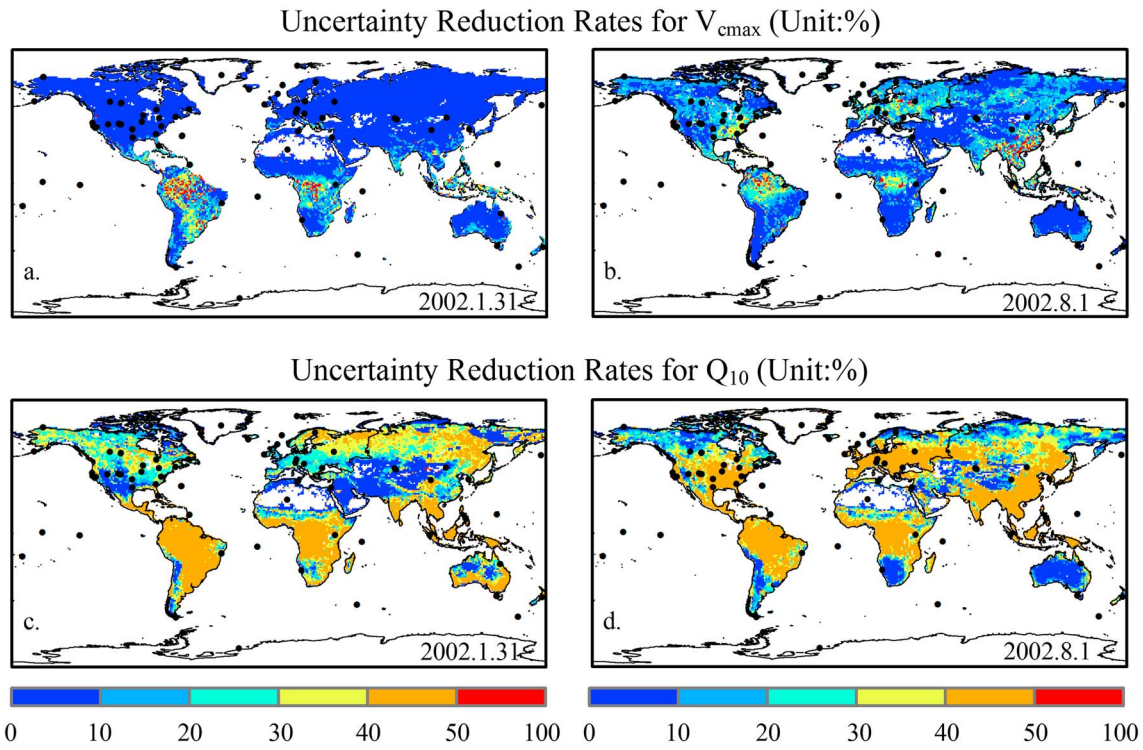

Figure 14. The distribution of uncertainty reduction rates of V_{max}^{25} and Q_{10} for one assimilation window. The black points are locations of CO_2 concentration observation sites. (a) The distribution of uncertainty reduction rates of V_{max}^{25} in 31 January 2002. (b) The distribution of uncertainty reduction rates of V_{max}^{25} in 1 August 2002. (c) The distribution of uncertainty reduction rates of Q_{10} in 31 January 2002. (d) The distribution of uncertainty reduction rates of Q_{10} in 1 August 2002.

nongrowing seasons. The seasonal variation patterns of V_{max}^{25} could be highly correlated with variations of leaf nitrogen content and leaf mass per area (Grassi et al., 2002; Han et al., 2004; Misson et al., 2006). In fact, variations of leaf nitrogen content are also correlated with variations of leaf mass per area (Reich et al., 1995; Reich & Walters, 1994). To find a possible explanation for the regular seasonal variation patterns of V_{max}^{25} shown in this study, the relationship between optimized V_{max}^{25} and LAI for individual PFTs was investigated (Figure 15). The large seasonal variations of optimized V_{max}^{25} and LAI are synchronized for evergreen conifers (Figure 15a), although the weekly values fluctuate due to uncertainties in the data assimilation. Two peaks were found in the series of optimized V_{max}^{25} for deciduous conifers, while only one peak was shown in the series of LAI data (Figure 15b). The peak of LAI lags the first peak of optimized V_{max}^{25}. The inconsistencies in the series of LAI and optimized V_{max}^{25} may be caused by lacking of observations in areas dominated by deciduous conifers. The seasonal curves of optimized V_{max}^{25} and LAI for broadleaf evergreen forests are reasonably smooth (Figure 15c). Growth/senescence of leaf area and increase/decrease in leaf photosynthetic capacity occur simultaneously in the yearly cycle, leading to the similar seasonal variation patterns between LAI and optimized V_{max}^{25} for midlatitude and high-latitude plant functional types. This broad pattern of synchronicity between LAI and V_{max}^{25} could be partly explained by the allocations of leaf nitrogen to Rubisco (Hrstka, Urban, & Babák, 2012; Wilson et al., 2000) and leaf chlorophyll pigments (Croft et al., 2017) that increase most rapidly in growing leaves or decrease rapidly in senescing leaves. So far there have been limited reports on the seasonal variations of leaf chlorophyll content and V_{max}^{25}. The results in this study suggest that this is an area deserving close attention in ground-based measurement programs.

One important result of this study is the spatial distribution and seasonal variation of V_{max}^{25} at the global scale. The result confirms the conclusions drawn by previous studies at leaf, canopy, or field scale. This is not just merely to show that results from GCAS agree with existing ones, but this is the first time to show that atmospheric CO_2 does have the information on the seasonal variation of this key photosynthetic parameter, and therefore, the V_{max}^{25} maps produced in this study would be a leap forward from limited ground points to

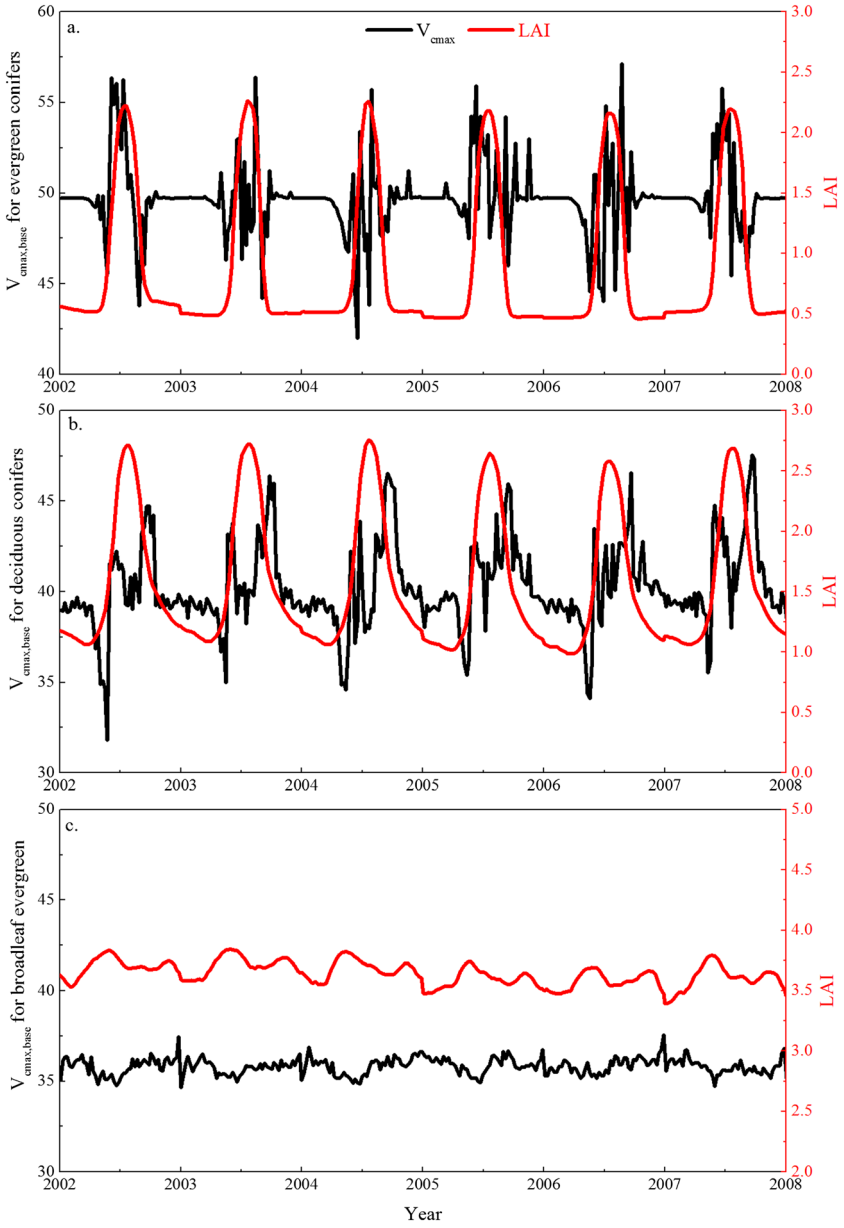

Figure 15. Time series of weekly optimized V_{max}^{25} and LAI for individual PFT during the period from 2002 to 2008. The red line is a time series of LAI. The black line is a time series of optimized V_{max}^{25}.

spatially and temporally cohesive patterns. The spatial pattern and seasonal variations of V_{max}^{25} may have implications for parameterization of the Farquhar's leaf-level model.

5.2. Errors in GCAS

Errors in an optimization study are due to a combination of three factors: a limited number of measurements, errors in prediction models, and errors in input data (Carvalhais et al., 2008). The limited number of measurements usually causes underdetermination problems in assimilation systems. In the case of CCDAS (Rayner et al., 2005), it optimized model parameters as averages for individual PFT to reduce the dimension of the state variables. In GCAS, there are about 26,000 parameters estimated in an assimilation window. The underdetermination problem is solved in GCAS in two steps. In the first step, regional fluxes (e.g., Transcom regions) can be constrained well using CO_2 concentration measurements, as shown by many previous atmospheric inversion studies (Peylin et al., 2013). A regional flux is the accumulation of fluxes from

all grids in the region. The contribution from every grid to the regional flux is different. Therefore, the regional flux retrieved from assimilation/inversion systems can be downscaled to the fine spatial resolution using information provided by the distribution of prior fluxes from TBMs. Since LAI data from remote sensing (Liu et al., 2012) were used as input to the BEPS model, the distribution of prior fluxes simulated by BEPS is reliable in terms of the spatial patterns of the fluxes. In this way, fluxes with a high spatial resolution could be optimized by a limited number of CO_2 concentration measurements (Zhang et al., 2014). In the second step, parameters can be estimated using the high resolution fluxes as observations at the fine spatial resolution in an assimilation system.

Ideally, each parameter should be optimized using independent observations. However, one type of observation is usually used to estimate more than one parameter due to lack of observations (Yuan et al., 2012). For instance, two or five parameters were determined from CO_2 flux observations using data assimilation techniques (He et al., 2014; Mo et al., 2008). Multiple years of CO_2 and water fluxes observations were used to estimate more than 10 parameters using nonlinear inversion methods (Braswell et al., 2005; Moore et al., 2008; Santaren et al., 2007; Wolf et al., 2006). Almost all parameter estimation studies use covariance matrixes of prediction models to determine a set of optimal parameters when observations are limited. As shown in Text S2, the sensitivities of parameters are estimated and contained in an error covariance matrix (e.g., P in equation (12)) to apportion model-data mismatches to various parameters. A larger sensitivity of the cost function to a given parameter indicates that this parameter is more adjusted than others, and the parameter with a larger sensitivity is therefore more tightly constrained by the measurements (Santaren et al., 2007). Like many previous studies, the error covariance matrixes for the prediction model (M), which represent sensitivities and correlations of NEP to V_{max}^{25} and Q_{10}, were used to provide the necessary information for optimizing these two parameters using only CO_2 concentration measurements in GCAS. The sensitivities of the CO_2 concentrations to photosynthetic and respiratory parameters are estimated based on the physical principles of BEPS. Models may not be reliable to estimate the magnitudes of various fluxes but may be far more reliable to estimate the sensitivities of the fluxes to key model parameters. Because of this, the partition of the total errors in simulating the CO_2 concentration at a given time into respiratory and photosynthetic flux errors is mostly credible. Nevertheless, more types of observations can be integrated into GCAS to reduce the impacts of the uncertainty in the sensitivities of parameters to one type of observation.

Furthermore, the errors from the prediction model also contribute errors to optimized results. The errors from the prediction model arise from parameter errors and model errors. In GCAS, only two parameters (V_{max}^{25} and Q_{10}) and the size of soil carbon pools are optimized. However, other parameters may also have contributed to the variations in CO_2 concentrations. The errors related to other parameters may be folded into the three parameters in GCAS. This means that the values V_{max}^{25} and Q_{10} optimized this way may be biased if other parameters of importance to photosynthesis and respiration have large errors. For the model errors, the forecast error matrixes of the prediction model (section 2.1) were estimated using a perturbed ensemble of model parameters under an ensemble Kalman filter (section 3.3). Since only one transport model is used in GCAS, the transport uncertainty is not evaluated. In fact, Stephens et al. (2007) indicated that errors in vertical transport contribute significantly to the seasonal errors of CO_2 concentration perditions. In future studies, these errors from transport models may be assessed using simulation experiments as done by Chevallier, Breon, and Rayner (2007). In addition, errors caused by simulations of the boundary layer height in the transport model also must be considered in the future. The height of the boundary layer is a critical parameter in atmospheric transport models, since it controls the extent of the vertical mixing of trace gases emitted near the surface (Koffi et al., 2016).

Finally, uncertainties in the forcing data also contribute to errors in GCAS. The optimized background fluxes from CT2013 were used as inputs to GCAS. The background CO_2 concentration distribution at the beginning of the optimization period (2002) was obtained through a 2 year transport model spin-up procedure. Although the errors from these background fluxes are mostly minimized by CT2013, the background fluxes also need to be optimized in GCAS in the future. In addition, errors from meteorological forcing data for BEPS and MOZART are also projected into the optimized parameters. For example, errors in temperature variation can be mapped into V_{max}^{25}, and uncertainties in precipitation can influence the optimized value of Q_{10} because soil moisture is not optimized in GCAS.

6. Conclusion

In this study, the Global Carbon Assimilation System (GCAS) is used to investigate the spatiotemporal variations of terrestrial ecosystem model parameters. The following conclusions are drawn:

1. The spatial patterns of V_{max}^{25} and Q_{10} are explored in this study. Mean values of optimized V_{max}^{25} for C4 plants, evergreen conifers forests, deciduous conifers forests, broadleaf evergreen forests, shrubs, and other types plants are 100.3, 62.5, 39.1, 28.8, 57.6, and 89.7 μmol m^{-2} s^{-1}, respectively. Vegetation from tropical zones has relatively lower V_{max}^{25} values than vegetation in temperate regions. Optimized multiyear average Q_{10} values varied from 1.95 to 2.05 over most regions of the world. Relatively high values of Q_{10} are derived over high/midlatitude regions.
2. Seasonal variations of V_{max}^{25} and Q_{10} are pronounced at middle and high latitudes in both hemispheres. The maximum V_{max}^{25} occurs during the growing season, while the minimum appears during the nongrowing season. Q_{10} values decreases with increasing temperature. The seasonal variability of V_{max}^{25} and Q_{10} are larger over high-latitude regions than over low-latitude regions.
3. The spatial distribution of the size of soil carbon pools optimized based on atmospheric CO_2 data improved the comparison with the gridded Global Soil Data Set for Earth System models retrieved from measurements, suggesting that the temporal variations of atmospheric CO_2 concentration contains information on the strength of heterotrophic respiration that can be effectively tapped through data assimilation techniques.

Acknowledgments
This work was supported by the National Key R&D Program of China (grant 2016YFA0600204) and the National Natural Science Foundation of China (grant 41571338). Readers can acquire the numerical outputs of GCAS through visiting the following address: http://globalchange.bnu.edu.cn/chen/. We want to thank Editor Ankur Desai and anonymous reviewers for their helpful and constructive comments.

References

Ali, A. A., Xu, C., Rogers, A., McDowell, N. G., Medlyn, B. E., Fisher, R. A., … Bauerle, W. L. (2015). Global-scale environmental control of plant photosynthetic capacity. *Ecological Applications*, *25*(8), 2349–2365.

Braswell, B. H., Sacks, W. J., Linder, E., & Schimel, D. S. (2005). Estimating diurnal to annual ecosystem parameters by synthesis of a carbon flux model with eddy covariance net ecosystem exchange observations. *Global Change Biology*, *11*(2), 335–355.

Carvalhais, N., Reichstein, M., Seixas, J., Collatz, G. J., Pereira, J. S., Berbigier, P., … Papale, D. (2008). Implications of the carbon cycle steady state assumption for biogeochemical modeling performance and inverse parameter retrieval. *Global Biogeochemical Cycles*, *22*, GB2007. https://doi.org/10.1029/2007GB003033

Chen, J. M., Ju, W. M., Cihlar, J., Price, D., Liu, J., Chen, W. J., … Barr, A. (2003). Spatial distribution of carbon sources and sinks in Canada's forests. *Tellus Series B: Chemical and Physical Meteorology*, *55*(2), 622–641. https://doi.org/10.1034/j.1600-0889.2003.00036.x

Chen, J. M., Liu, J., Cihlar, J., & Goulden, M. L. (1999). Daily canopy photosynthesis model through temporal and spatial scaling for remote sensing applications. *Ecological Modelling*, *124*(2–3), 99–119. https://doi.org/10.1016/s0304-3800(99)00156-8

Chen, J. M., Mo, G., Pisek, J., Liu, J., Deng, F., Ishizawa, M., & Chan, D. (2012). Effects of foliage clumping on the estimation of global terrestrial gross primary productivity. *Global Biogeochemical Cycles*, *26*, GB1019. https://doi.org/10.1029/2010GB003996

Chen, Z., Chen, J. M., Zheng, X., Jiang, F., Qin, J., Zhang, S., … Mo, G. (2015). Optimizing photosynthetic and respiratory parameters based on the seasonal variation pattern in regional net ecosystem productivity obtained from atmospheric inversion. *Chinese Science Bulletin*, *60*(22), 1954–1961.

Chevallier, F., Breon, F. M., & Rayner, P. J. (2007). Contribution of the Orbiting Carbon Observatory to the estimation of CO_2 sources and sinks: Theoretical study in a variational data assimilation framework. *Journal of Geophysical Research*, *112*, D09307. https://doi.org/10.1029/2006JD007375

Chevallier, F., Ciais, P., Conway, T. J., Aalto, T., Anderson, B. E., Bousquet, P., … Worthy, D. (2010). CO_2 surface fluxes at grid point scale estimated from a global 21 year reanalysis of atmospheric measurements. *Journal of Geophysical Research*, *115*, D21307. https://doi.org/10.1029/2010JD013887

Croft, H., Chen, J., Froelich, N., Chen, B., & Staebler, R. (2015). Seasonal controls of canopy chlorophyll content on forest carbon uptake: Implications for GPP modeling. *Journal of Geophysical Research: Biogeosciences*, *120*, 1576–1,586. https://doi.org/10.1002/2015JG002980

Croft, H., Chen, J. M., Luo, X., Barlett, P., Chen, B., & Staebler, R. (2017). Leaf chlorophyll content as a proxy for leaf photosynthetic capacity. *Global Change Biology*, *23*, 3513–3524.

De Kauwe, M. G., Lin, Y. S., Wright, I. J., Medlyn, B. E., Crous, K. Y., Ellsworth, D. S., … Rogers, A. (2015). A test of the 'one-point method' for estimating maximum carboxylation capacity from field-measured, light-saturated photosynthesis. *New Phytologist*, *210*, 1130–1144. https://doi.org/10.1111/nph.13815

Dolman, A., Shvidenko, A., Schepaschenko, D., Ciais, P., Tchebakova, N., Chen, T., … Maksyutov, S. (2012). An estimate of the terrestrial carbon budget of Russia using inventory-based, eddy covariance and inversion methods. *Biogeosciences*, *9*(12), 5323–5340.

Emmons, L., Walters, S., Hess, P., Lamarque, J.-F., Pfister, G., Fillmore, D., … Laepple, T. (2010). Description and evaluation of the Model for Ozone and Related chemical Tracers, version 4 (MOZART-4). *Geoscientific Model Development*, *3*(1), 43–67.

Enting, I. G., & Mansbridge, J. V. (1989). Seasonal sources and sinks of atmospheric CO(2) direct inversion of filtered data. *Tellus Series B: Chemical and Physical Meteorology*, *41*(2), 111–126. https://doi.org/10.1111/j.1600-0889.1989.tb00129.x

Farquhar, G. D., Caemmerer, S. V., & Berry, J. A. (1980). A biochemical model of photosynthetic CO_2 assimilation in leaves of C_3 species. *Planta*, *149*(1), 78–90. https://doi.org/10.1007/bf00386231

Grassi, G., Meir, P., Cromer, R., Tompkins, D., & Jarvis, P. (2002). Photosynthetic parameters in seedlings of *Eucalyptus grandis* as affected by rate of nitrogen supply. *Plant, Cell & Environment*, *25*(12), 1677–1688.

Green, E. J., MacFarlane, D. W., Valentine, H. T., & Strawderman, W. E. (1999). Assessing uncertainty in a stand growth model by Bayesian synthesis. *Forest Science*, *45*(4), 528–538.

Gurney, K. R., Baker, D., Rayner, P., & Denning, S. (2008). Interannual variations in continental-scale net carbon exchange and sensitivity to observing networks estimated from atmospheric CO(2) inversions for the period 1980 to 2005. *Global Biogeochemical Cycles*, *22*, GB3025. https://doi.org/10.1029/2007GB003082

Gurney, K. R., Law, R. M., Denning, A. S., Rayner, P. J., Pak, B. C., Baker, D., … Ciais, P. (2004). Transcom 3 inversion intercomparison: Model mean results for the estimation of seasonal carbon sources and sinks. *Global Biogeochemical Cycles*, *18*, GB1010. https://doi.org/10.1029/2003GB002111

Han, Q., Kawasaki, T., Nakano, T., & Chiba, Y. (2004). Spatial and seasonal variability of temperature responses of biochemical photosynthesis parameters and leaf nitrogen content within a *Pinus densiflora* crown. *Tree Physiology*, *24*(7), 737–744.

He, L., Chen, J. M., Liu, J., Mo, G., Bélair, S., Zheng, T., … Arain, M. A. (2014). Optimization of water uptake and photosynthetic parameters in an ecosystem model using tower flux data. *Ecological Modelling*, *294*, 94–104.

Hikosaka, K., Ishikawa, K., Borjigidai, A., Muller, O., & Onoda, Y. (2006). Temperature acclimation of photosynthesis: Mechanisms involved in the changes in temperature dependence of photosynthetic rate. *Journal of Experimental Botany*, *57*(2), 291–302.

Hrstka, M., Urban, O., & Babák, L. (2012). Seasonal changes of Rubisco content and activity in *Fagus sylvatica* and *Picea abies* affected by elevated CO_2 concentration. *Chemical Papers*, *66*(9), 836–841.

Jacobson, A. R., Mikaloff Fletcher, S. E., Gruber, N., Sarmiento, J. L., & Gloor, M. (2007). A joint atmosphere-ocean inversion for surface fluxes of carbon dioxide: 1. Methods and global-scale fluxes. *Global Biogeochemical Cycles*, *21*, GB1019. https://doi.org/10.1029/2005GB002556

Janssens, I. A., & Pilegaard, K. (2003). Large seasonal changes in Q10 of soil respiration in a beech forest. *Global Change Biology*, *9*(6), 911–918.

Ju, W., Chen, J. M., Black, T. A., Barr, A. G., Liu, J., & Chen, B. (2006). Modelling multi-year coupled carbon and water fluxes in a boreal aspen forest. *Agricultural and Forest Meteorology*, *140*(1-4), 136–151. https://doi.org/10.1016/j.agrformet.2006.08.008

Kalnay, E., Kanamitsu, M., Kistler, R., Collins, W., Deaven, D., Gandin, L., … Joseph, D. (1996). The NCEP/NCAR 40-year reanalysis project. *Bulletin of the American Meteorological Society*, *77*(3), 437–471. https://doi.org/10.1175/1520-0477(1996)077%3C0437:tnyrp%3E2.0.co;2

Kaminski, T., Knorr, W., Rayner, P. J., & Heimann, M. (2002). Assimilating atmospheric data into a terrestrial biosphere model: A case study of the seasonal cycle. *Global Biogeochemical Cycles*, *16*(4), 1066. https://doi.org/10.1029/2001GB001463

Kaminski, T., Knorr, W., Scholze, M., Gobron, N., Pinty, B., Giering, R., & Mathieu, P. P. (2012). Consistent assimilation of MERIS FAPAR and atmospheric CO_2 into a terrestrial vegetation model and interactive mission benefit analysis. *Biogeosciences*, *9*(8), 3173–3184. https://doi.org/10.5194/bg-9-3173-2012

Kaminski, T., Knorr, W., Schürmann, G., Scholze, M., Rayner, P. J., Zaehle, S., … Ziehn, T. (2013). The BETHY/JSBACH carbon cycle data assimilation system: Experiences and challenges. *Journal of Geophysical Research: Biogeosciences*, *118*, 1414–1426. https://doi.org/10.1002/jgrg.20118

Kaminski, T., Rayner, P. J., Vossbeck, M., Scholze, M., & Koffi, E. (2012). Observing the continental-scale carbon balance: Assessment of sampling complementarity and redundancy in a terrestrial assimilation system by means of quantitative network design. *Atmospheric Chemistry and Physics*, *12*(16), 7867–7879. https://doi.org/10.5194/acp-12-7867-2012

Kaminski, T., Scholze, M., & Houweling, S. (2010). Quantifying the benefit of A-SCOPE data for reducing uncertainties in terrestrial carbon fluxes in CCDAS. *Tellus Series B: Chemical and Physical Meteorology*, *62*(5), 784–796. https://doi.org/10.1111/j.1600-0889.2010.00483.x

Kato, T., Knorr, W., Scholze, M., Veenendaal, E., Kaminski, T., Kattge, J., & Gobron, N. (2013). Simultaneous assimilation of satellite and eddy covariance data for improving terrestrial water and carbon simulations at a semi-arid woodland site in Botswana. *Biogeosciences*, *10*(2), 789–802. https://doi.org/10.5194/bg-10-789-2013

Kattge, J., & Knorr, W. (2007). Temperature acclimation in a biochemical model of photosynthesis: A reanalysis of data from 36 species. *Plant, Cell & Environment*, *30*(9), 1,176–1,190.

Kattge, J., Knorr, W., Raddatz, T., & Wirth, C. (2009). Quantifying photosynthetic capacity and its relationship to leaf nitrogen content for global-scale terrestrial biosphere models. *Global Change Biology*, *15*(4), 976–991. https://doi.org/10.1111/j.1365-2486.2008.01744.x

Kirschbaum, M. U. F. (1995). The temperature dependence of soil organic matter decomposition, and the effect of global warming on soil organic C storage. *Soil Biology & Biochemistry*, *27*(6), 753–760. https://doi.org/10.1016/0038-0717(94)00242-s

Kirschbaum, M. U. F. (2010). The temperature dependence of organic matter decomposition: Seasonal temperature variations turn a sharp short-term temperature response into a more moderate annually averaged response. *Global Change Biology*, *16*(7), 2117–2129. https://doi.org/10.1111/j.1365-2486.2009.02093.x

Knorr, W. (2000). Annual and interannual CO_2 exchanges of the terrestrial biosphere: Process-based simulations and uncertainties. *Global Ecology and Biogeography*, *9*(3), 225–252. https://doi.org/10.1046/j.1365-2699.2000.00159.x

Knorr, W., & Heimann, M. (2001a). Uncertainties in global terrestrial biosphere modeling 1. A comprehensive sensitivity analysis with a new photosynthesis and energy balance scheme. *Global Biogeochemical Cycles*, *15*, 207–225. https://doi.org/10.1029/1998GB001059

Knorr, W., & Heimann, M. (2001b). Uncertainties in global terrestrial biosphere modeling, Part II: Global constraints for a process-based vegetation model. *Global Biogeochemical Cycles*, *15*, 227–246. https://doi.org/10.1029/1998GB001060

Knorr, W., Kaminski, T., Scholze, M., Gobron, N., Pinty, B., Giering, R., & Mathieu, P. P. (2010). Carbon cycle data assimilation with a generic phenology model. *Journal of Geophysical Research*, *115*, G04017. https://doi.org/10.1029/2009JG001119

Koffi, E. N., Bergamaschi, P., Karstens, U., Krol, M., Segers, A., Schmidt, M., … Kazan, V. (2016). Evaluation of the boundary layer dynamics of the TM5 model over Europe. *Geoscientific Model Development*, *9*(9), 3137.

Koffi, E. N., Rayner, P. J., Scholze, M., & Beer, C. (2012). Atmospheric constraints on gross primary productivity and net ecosystem productivity: Results from a carbon-cycle data assimilation system. *Global Biogeochemical Cycles*, *26*, GB1024. https://doi.org/10.1029/2010GB003900

Koffi, E. N., Rayner, P. J., Scholze, M., Chevallier, F., & Kaminski, T. (2013). Quantifying the constraint of biospheric process parameters by CO_2 concentration and flux measurement networks through a carbon cycle data assimilation system. *Atmospheric Chemistry and Physics*, *13*(21), 10,555–10,572. https://doi.org/10.5194/acp-13-10555-2013

Krinner, G., Viovy, N., de Noblet-Ducoudre, N., Ogee, J., Polcher, J., Friedlingstein, P., … Prentice, I. C. (2005). A dynamic global vegetation model for studies of the coupled atmosphere-biosphere system. *Global Biogeochemical Cycles*, *19*, GB1015. https://doi.org/10.1029/2003GB002199

Kuppel, S., Chevallier, F., & Peylin, P. (2013). Quantifying the model structural error in carbon cycle data assimilation systems. *Geoscientific Model Development*, *6*(1), 45–55. https://doi.org/10.5194/gmd-6-45-2013

Le Quere, C., Andres, R., Boden, T., Conway, T., Houghton, R. A., House, J. I., … Zeng, N. (2013). The global carbon budget 1959–2011. *Earth System Science Data*, *5*, 165–185.

Le Quéré, C., Peters, G., Andres, R., Andrew, T. A., Boden, P., Ciais, P., … Zaehle, S. (2014). Global carbon budget 2013. *Earth System Science Data*, *6*, 235–263.

Liu, Y., Liu, R., & Chen, J. M. (2012). Retrospective retrieval of long-term consistent global leaf area index (1981–2011) from combined AVHRR and MODIS data. *Journal of Geophysical Research*, *117*, G04003. https://doi.org/10.1029/2012JG002084

Lloyd, J., & Taylor, J. (1994). On the temperature dependence of soil respiration. *Functional Ecology*, 315–323.

Luo, Y. Q., White, L. W., Canadell, J. G., DeLucia, E. H., Ellsworth, D. S., Finzi, A. C., … Schlesinger, W. H. (2003). Sustainability of terrestrial carbon sequestration: A case study in Duke Forest with inversion approach. *Global Biogeochemical Cycles*, *17*, 1021. https://doi.org/10.1029/2002GB001923

Mahecha, M. D., Reichstein, M., Carvalhais, N., Lasslop, G., Lange, H., Seneviratne, S. I., … Richardson, A. (2010). Global convergence in the temperature sensitivity of respiration at ecosystem level. *Science*, *329*(5993), 838–840.

Marland, G., Boden, T., Andres, R., Brenkert, A., & Johnston, C. (2007). Global, regional, and national fossil fuel CO_2 emissions, Trends: A Compendium of Data on Global Change (pp. 37,831–36,335).

Masarie, K., Peters, W., Jacobson, A., & Tans, P. (2014). ObsPack: A framework for the preparation, delivery, and attribution of atmospheric greenhouse gas measurements. *Earth System Science Data*, *6*(2), 375–384.

Medlyn, B., Badeck, F. W., De Pury, D., Barton, C., Broadmeadow, M., Ceulemans, R., … Kellomäki, S. (1999). Effects of elevated CO_2 on photosynthesis in European forest species: A meta-analysis of model parameters, Plant. *Cell & Environment*, *22*(12), 1475–1495.

Medlyn, B., Dreyer, E., Ellsworth, D., Forstreuter, M., Harley, P., Kirschbaum, M., … Walcroft, A. (2002). Temperature response of parameters of a biochemically based model of photosynthesis. II. A review of experimental data. *Plant, Cell & Environment*, *25*(9), 1167–1179.

Misson, L., Tu, K. P., Boniello, R. A., & Goldstein, A. H. (2006). Seasonality of photosynthetic parameters in a multi-specific and vertically complex forest ecosystem in the Sierra Nevada of California. *Tree Physiology*, *26*(6), 729–741.

Mo, X., Chen, J. M., Ju, W., & Black, T. A. (2008). Optimization of ecosystem model parameters through assimilating eddy covariance flux data with an ensemble Kalman filter. *Ecological Modelling*, *217*(1-2), 157–173. https://doi.org/10.1016/j.ecolmodel.2008.06.021

Moore, D. J., Hu, J., Sacks, W. J., Schimel, D. S., & Monson, R. K. (2008). Estimating transpiration and the sensitivity of carbon uptake to water availability in a subalpine forest using a simple ecosystem process model informed by measured net CO2 and H 2 O fluxes. *Agricultural and Forest Meteorology*, *148*(10), 1467–1477.

Niinemets, Ü., Keenan, T. F., & Hallik, L. (2015). A worldwide analysis of within-canopy variations in leaf structural, chemical and physiological traits across plant functional types. *New Phytologist*, *205*(3), 973–993.

Oda, T., & Maksyutov, S. (2011). A very high-resolution (1 km × 1 km) global fossil fuel CO2 emission inventory derived using a point source database and satellite observations of nighttime lights. *Atmospheric Chemistry and Physics*, *11*(2), 543–556.

Peters, W., Jacobson, A. R., Sweeney, C., Andrews, A. E., Conway, T. J., & Masarie, K. (2007). An atmospheric perspective on North American carbon dioxide exchange: CarbonTracker. *Proceedings of the National Academy of Sciences of the United States of America*, *104*(48), 18,925–18,930. https://doi.org/10.1073/pnas.0708986104

Peters, W., Krol, M. C., Van Der Werf, G. R., Houweling, S., Jones, C. D., Hughes, J., … Tans, P. P. (2010). Seven years of recent European net terrestrial carbon dioxide exchange constrained by atmospheric observations. *Global Change Biology*, *16*(4), 1317–1337. https://doi.org/10.1111/j.1365-2486.2009.02078.x

Peylin, P., Law, R. M., Gurney, K. R., Chevallier, F., Jacobson, A. R., Maki, T., … Zhang, X. (2013). Global atmospheric carbon budget: Results from an ensemble of atmospheric CO_2 inversions. *Biogeosciences*, *10*(10), 6699–6720. https://doi.org/10.5194/bg-10-6699-2013

Potter, C. S., Randerson, J. T., Field, C. B., Matson, P. A., Vitousek, P. M., Mooney, H. A., & Klooster, S. A. (1993). Terrestrial ecosystem production: A process model based on global satellite and surface data. *Global Biogeochemical Cycles*, *7*, 811–841. https://doi.org/10.1029/93gb02725

Rayner, P. J., Law, R. M., Allison, C. E., Francey, R. J., Trudinger, C. M., & Pickett-Heaps, C. (2008). Interannual variability of the global carbon cycle (1992–2005) inferred by inversion of atmospheric CO_2 and delta(CO_2)-C_{13} measurements. *Global Biogeochemical Cycles*, *22*, GB3008. https://doi.org/10.1029/2007gb003068

Rayner, P. J., Scholze, M., Knorr, W., Kaminski, T., Giering, R., & Widmann, H. (2005). Two decades of terrestrial carbon fluxes from a carbon cycle data assimilation system (CCDAS). *Global Biogeochemical Cycles*, *19*, GB2026. https://doi.org/10.1029/2004gb002254

Reich, P., & Walters, M. (1994). Photosynthesis-nitrogen relations in Amazonian tree species. II. Variation in nitrogen vis-a-vis specific leaf area influences mass-and area-based expressions. *Oecologia*, *97*, 73–81.

Reich, P., Walters, M., Kloeppel, B., & Ellsworth, D. (1995). Different photosynthesis-nitrogen relations in deciduous hardwood and evergreen coniferous tree species. *Oecologia*, *104*(1), 24–30.

Reich, P. B., Wright, I. J., & Lusk, C. H. (2007). Predicting leaf physiology from simple plant and climate attributes: A global GLOPNET analysis. *Ecological Applications*, *17*(7), 1982–1988.

Rodenbeck, C., Houweling, S., Gloor, M., & Heimann, M. (2003). Time-dependent atmospheric CO_2 inversions based on interannually varying tracer transport. *Tellus Series B: Chemical and Physical Meteorology*, *55*(2), 488–497. https://doi.org/10.1034/j.1600-0889.2003.00033.x

Santaren, D., Peylin, P., Viovy, N., & Ciais, P. (2007). Optimizing a process-based ecosystem model with eddy-covariance flux measurements: A pine forest in southern France. *Global Biogeochemical Cycles*, *21*, GB2013. https://doi.org/10.1029/2006GB002834

Shangguan, W., Dai, Y., Duan, Q., Liu, B., & Yuan, H. (2014). A global soil data set for earth system modeling. *Journal of Advances in Modeling Earth Systems*, *6*(1), 249–263. https://doi.org/10.1002/2013ms000293

Sitch, S., Smith, B., Prentice, I. C., Arneth, A., Bondeau, A., Cramer, W., … Venevsky, S. (2003). Evaluation of ecosystem dynamics, plant geography and terrestrial carbon cycling in the LPJ dynamic global vegetation model. *Global Change Biology*, *9*(2), 161–185. https://doi.org/10.1046/j.1365-2486.2003.00569.x

Stephens, B. B., Gurney, K. R., Tans, P. P., Sweeney, C., Peters, W., Bruhwiler, L. M. P., … Nakazawa, T. (2007). Weak northern and strong tropical land carbon uptake from vertical profiles of atmospheric CO_2. *Science*, *316*(5832), 1732–1735.

Takahashi, T., Sutherland, S. C., Wanninkhof, R., Sweeney, C., Feely, R. A., Chipman, D. W., … Sabine, C. (2009). Climatological mean and decadal change in surface ocean pCO2, and net sea-air CO 2 flux over the global oceans. *Deep Sea Research Part II: Topical Studies in Oceanography*, *56*(8), 554–577.

Tans, P. P., Conway, T. J., & Nakazawa, T. (1989). Latitudinal distribution of the sources and sinks of atmospheric carbon dioxide derived from surface observations and an atmospheric transport model. *Journal of Geophysical Research*, *94*, 5151–5172. https://doi.org/10.1029/JD094iD04p05151

van der Werf, G. R., Randerson, J. T., Giglio, L., Collatz, G. J., Kasibhatla, P. S., & Arellano, A. F. Jr. (2006). Interannual variability in global biomass burning emissions from 1997 to 2004. *Atmospheric Chemistry and Physics*, *6*, 3423–3441.

Wang, Y.-P., Baldocchi, D., Leuning, R., Falge, E., & Vesala, T. (2007). Estimating parameters in a land-surface model by applying nonlinear inversion to eddy covariance flux measurements from eight FLUXNET sites. *Global Change Biology*, *13*(3), 652–670. https://doi.org/10.1111/j.1365-2486.2006.01225.x

Wang, Y.-P., & Leuning, R. (1998). A two-leaf model for canopy conductance, photosynthesis and partitioning of available energy I: Model description and comparison with a multi-layered model. *Agricultural and Forest Meteorology*, *91*(1-2), 89–111. https://doi.org/10.1016/s0168-1923(98)00061-6

Wang, Y.-P., Trudinger, C. M., & Enting, I. G. (2009). A review of applications of model-data fusion to studies of terrestrial carbon fluxes at different scales. *Agricultural and Forest Meteorology*, *149*(11), 1829–1842. https://doi.org/10.1016/j.agrformet.2009.07.009

Wilson, K. B., Baldocchi, D. D., & Hanson, P. J. (2000). Spatial and seasonal variability of photosynthetic parameters and their relationship to leaf nitrogen in a deciduous forest. *Tree Physiology*, *20*(9), 565–578.

Wolf, A., Akshalov, K., Saliendra, N., Johnson, D. A., & Laca, E. A. (2006). Inverse estimation of Vcmax, leaf area index, and the Ball-Berry parameter from carbon and energy fluxes. *Journal of Geophysical Research*, *111*, D08S08. https://doi.org/10.1029/2005JD005927

Yamori, W., Noguchi, K., & Terashima, I. (2005). Temperature acclimation of photosynthesis in spinach leaves: Analyses of photosynthetic components and temperature dependencies of photosynthetic partial reactions. *Plant, Cell & Environment*, *28*(4), 536–547.

Yuan, W., Liang, S., Liu, S., Weng, E., Luo, Y., Hollinger, D., & Zhang, H. (2012). Improving model parameter estimation using coupling relationships between vegetation production and ecosystem respiration. *Ecological Modelling*, *240*, 29–40.

Zhang, S., Yi, X., Zheng, X., Chen, Z., Dan, B., & Zhang, X. (2014). Global carbon assimilation system using a local ensemble Kalman filter with multiple ecosystem models. *Journal of Geophysical Research: Biogeosciences*, *119*, 2171–2187. https://doi.org/10.1002/2014JG002792

Zhang, S., Zheng, X., Chen, J. M., Chen, Z., Dan, B., Yi, X., … Wu, G. (2015). A global carbon assimilation system using a modified ensemble Kalman filter. *Geoscientific Model Development*, *8*(3), 805–816. https://doi.org/10.5194/gmd-8-805-2015

Zheng, H., Li, Y., Chen, J., Wang, T., Huang, Q., & Sheng, Y. (2014). Applying a dual optimization method to quantify carbon fluxes: Recent progress in carbon flux inversion. *Chinese Science Bulletin*, *59*(2), 222–226. https://doi.org/10.1007/s11434-013-0016-5

Zheng, H., Li, Y., Chen, J. M., Wang, T., Huang, Q., Huang, W. X., … Jiang, F. (2015). A global carbon assimilation system based on a dual optimization method. *Biogeosciences*, *12*(4), 1131–1150. https://doi.org/10.5194/bg-12-1131-2015

Zhou, T., Shi, P., Hui, D., & Luo, Y. (2009). Global pattern of temperature sensitivity of soil heterotrophic respiration (Q_{10}) and its implications for carbon-climate feedback. *Journal of Geophysical Research*, *114*, G02016. https://doi.org/10.1029/2008JG000850

Ziehn, T., Knorr, W., & Scholze, M. (2011). Investigating spatial differentiation of model parameters in a carbon cycle data assimilation system. *Global Biogeochemical Cycles*, *25*, GB2021. https://doi.org/10.1029/2010GB003886

Ziehn, T., Scholze, M., & Knorr, W. (2011). Development of an ensemble-adjoint optimization approach to derive uncertainties in net carbon fluxes. *Geoscientific Model Development*, *4*(4), 1011–1018. https://doi.org/10.5194/gmd-4-1011-2011

Ziehn, T., Scholze, M., & Knorr, W. (2012). On the capability of Monte Carlo and adjoint inversion techniques to derive posterior parameter uncertainties in terrestrial ecosystem models. *Global Biogeochemical Cycles*, *26*, GB3025. https://doi.org/10.1029/2011GB004185

Zupanski, D., & Zupanski, M. (2006). Model error estimation employing an ensemble data assimilation approach. *Monthly Weather Review*, *134*(5), 1337–1354.